



**HAL**  
open science

## Transient absorption in inorganic systems

Minh-Huong Ha-Thi, Gotard Burdzinski, Thomas Pino, Pascale Changenet

► **To cite this version:**

Minh-Huong Ha-Thi, Gotard Burdzinski, Thomas Pino, Pascale Changenet. Transient absorption in inorganic systems. Springer Handbook of Inorganic Chemistry, In press, 10.1007/978-3-030-63713-2\_5 . hal-02991509

**HAL Id: hal-02991509**

**<https://hal.science/hal-02991509>**

Submitted on 10 Nov 2020

**HAL** is a multi-disciplinary open access archive for the deposit and dissemination of scientific research documents, whether they are published or not. The documents may come from teaching and research institutions in France or abroad, or from public or private research centers.

L'archive ouverte pluridisciplinaire **HAL**, est destinée au dépôt et à la diffusion de documents scientifiques de niveau recherche, publiés ou non, émanant des établissements d'enseignement et de recherche français ou étrangers, des laboratoires publics ou privés.

## Transient absorption spectroscopy in inorganic systems

Minh-Huong Ha-Thi,<sup>1</sup> Gotard Burdzinski,<sup>2</sup> Thomas Pino,<sup>1</sup> Pascale Changenet<sup>3</sup>

<sup>1</sup>Université Paris-Saclay, CNRS, Institut des Sciences Moléculaires d'Orsay, 91405, Orsay, France

<sup>2</sup>Faculty of Physics, Adam Mickiewicz University in Poznan, Poznan, Poland

<sup>3</sup>Laboratoire d'Optique et Biosciences, CNRS, INSERM, Ecole polytechnique, Institut Polytechnique de Paris, 91128 Palaiseau cedex, France

## Contents

List of Abbreviations .....	2
Abstract.....	3
1. General Introduction .....	3
2. Experimental techniques: basics .....	8
2.1. Nanosecond transient absorption technique .....	9
2.2. Femtosecond transient absorption technique .....	13
3. Latest instrumental developments.....	19
3.1 Pump-pump-probe .....	19
3.2 Basic principles of time-resolved electronic circular dichroism .....	21
3.3 Transient absorption spectroelectrochemistry .....	22
4. Applications .....	23
4.1. Pump-probe experiments .....	23
4.2. Multiple-charge photo-accumulation by pump-pump-probe experiments:.....	26
4.3. Combination of transient absorption and electrochemistry .....	29
4.4. Ruthenium complexes as chiral paradigms for TR-CD spectroscopy.....	31
5. Concluding remarks .....	33
References .....	33

# List of Abbreviations

CD	Circular Dichroism
CSS	Charge Separated State
DADS	Differential Decay Associated Spectra
ESA	Excited State Absorption
GSB	Ground State Bleaching
GVD	Group Velocity Dispersion
ICCD	Intensified Charge Coupled Device
IRF	Instrumental Response Function
LED	Light Emitting Diode
MLCT	Metal-to-Ligand Charge Transfer
OPO	Optical Parametric Oscillator
SAS	Species Associated Spectra
SE	Stimulated Emission
SEC	Spectroelectrochemistry
TA	Transient Absorption
TPA	Two-Photon Absorption

## Abstract

Transient absorption spectroscopy is one of the most popular methods to study photochemistry and photophysics. This technique allows observation of the dynamics in the electronic excited states after photoexcitation over a wide range of timescales, from the femtosecond to the millisecond timescales. The probed relaxation dynamics involve multiple channels in competition, such as internal conversion, intersystem crossing, fluorescence, energy transfer, electron transfer, proton-coupled electron transfer, chemical reactions, etc. The aim of this chapter is to provide general background and discuss state-of-the-art experimental techniques for transient absorption measurements. This will be illustrated by recent applications to study photoinduced processes in inorganic systems including molecular and hybrid systems, in particular toward renewable energy applications. Desirable developments, by no means exhaustive, will then be discussed to sustain future research.

**Keywords:** transient absorption spectroscopy, time-resolved spectroscopies, ultrafast, flash photolysis, pump-probe, relaxation dynamics, excited state, photophysical processes, photoinduced electron transfer, photocatalysis.

### 1. General Introduction

Light is an important vector of information. In nature, light can be converted into electrical, mechanical or chemical energy. Some well-known phenomena are visual transduction in mammals, photosynthesis in plants and photomovement in bacteria. The study of these natural photochemical processes has recently become of great interest for the development of sustainable sources of energy. Over the past century, the study of photochemical reactions has become an important goal of contemporary chemistry leading to a wide variety of applications ranging from Physics to Medicine. Notably, many industrial applications rely on photochemistry, such as photography, photocatalysis or photolithography. In medicine, phototherapy has been used for many decades for the treatment of jaundice for newborns, or skin disorders such as psoriasis or eczema, and more recently in the treatments of some cancers.

While thermal reactions take place from the fundamental electronic state of molecules upon heat activation, photochemical reactions occur from their excited electronic state produced by photon absorption. Photochemical reactions are thus highly selective and make it possible to obtain reaction products which are thermally inaccessible. Absorption of a photon by a molecule can cause photophysical and photochemical processes. Photophysical processes which cause no chemical change include radiative and non-radiative processes as illustrated by Perrin-Jablonski diagram (Figure 1). Photochemical processes concern interaction of light with molecules leading to a chemical reaction.

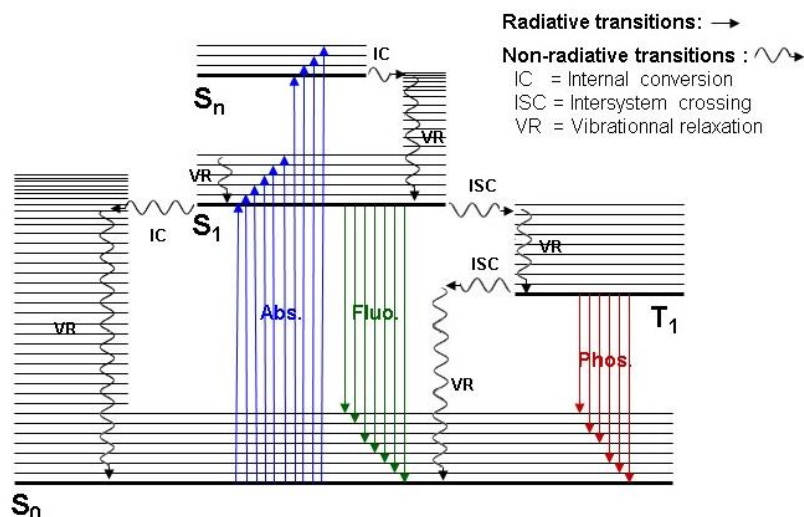


Figure 1. Perrin (1929)-Jablonski (1935) diagram for a closed-shell molecule in solution.

The competition between photophysical and photochemical processes implies that for a photochemical reaction to be efficient, it must be fast. Figure 2 illustrates the typical time scales of photophysical and photochemical processes in solution. Observation of these fast events requires time-resolved spectroscopic methods able to capture the different reaction intermediates of photoinduced processes. Among them, pump-probe methods are powerful techniques capable of detecting intermediate species formed after electronic excitation over time scales spanning from femtoseconds up to milliseconds. Pump-probe experiments take place in two steps. The first one, denoted the “pumping” step, consists in irradiating molecules with a short and strong flash of light in order to create a non-negligible population of electronic excited states. The second step consists in probing those unstable states by measuring the temporal variation in the intensity of a second weak light beam, which can be continuous or pulsed.

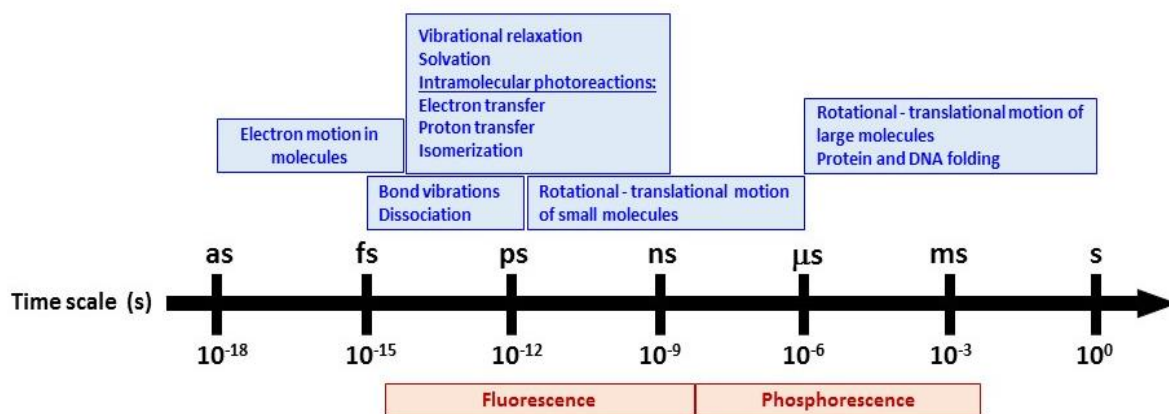


Figure 2. Typical time scales of photophysical and photochemical processes occurring in solution.

Development of pump-probe techniques started in the middle of the 20<sup>th</sup> century with the pioneering works of Norrish and Porter (Nobel prize in Chemistry, 1967), who built the first flash photolysis setup for studying kinetics of triplet-state reactivity and free

radicals[1-3]. Flash photolysis is a pump-probe method that originally used fast flash lamps seeded by huge capacitors to excite samples, providing a time resolution of about one microsecond. Flash photolysis has now become routine experiments. By using laser pulse excitation (Figure 3), a nanosecond time resolution can be easily attained.

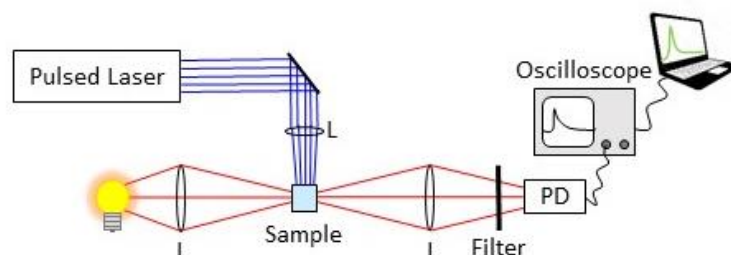


Figure 3. Basic principle of nanosecond-millisecond flash photolysis.

Time resolution of flash photolysis is mainly limited by laser pulse duration and detection and is typically slightly better than 10 ns. Characterization of photochemical processes on ultrafast time scales, *i.e.* in the femtosecond regime, requires all-optical pump-probe methods generally using one amplified ultrafast laser source to generate the pump and the probe. In this case, the temporal evolution of the excited-state population is measured by introducing an optical delay between the pump and the probe ( $\Delta x = 30 \mu\text{m}$  corresponds to  $\Delta t = 100 \text{ fs}$ ), as illustrated in Figure 4. The time resolution of such experiments depends mainly on the duration of the pump and probe pulses, *i.e.* the pump-probe correlation function. With the development of commercial femtosecond Ti:Sapphire laser sources from the 1990s, ultrafast transient absorption setups have now become widespread in laboratories. The development of ultrafast pump-probe spectroscopy took place at the interface of Physics and Chemistry and has been awarded several Nobel Prizes: N. Bloembergen and A. L. Schawlow, in 1981, for the development of laser spectroscopy [4, 5]; Zewail in 1999 for the development of femtochemistry [6]; D. Strickland and G. Mourou, in 2018, for the development of the chirped pulses amplification for the generation of high power femtosecond pulses [7].

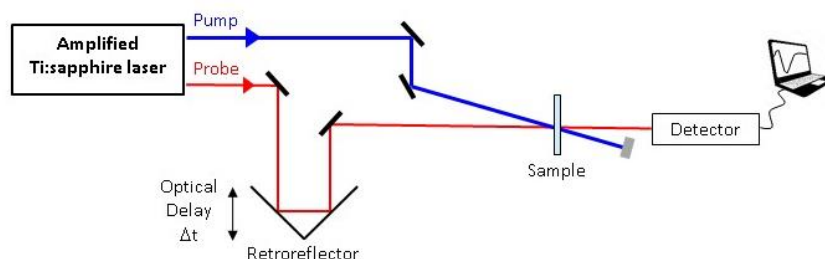


Figure 4. Basic principle of femtosecond transient absorption.

Practically, pump-probe or transient absorption experiments consist in measuring the intensity of the probe beam transmitted by the sample with and without the pump, for different pump-probe delays  $\Delta t$  at a given wavelength  $\lambda$ . The measured signals are usually expressed as the differential absorbance of the sample with and without the pump,  $A_p$  and  $A_{np}$ , respectively:

$$\Delta A(\lambda, \Delta t) = A_p(\lambda, \Delta t) - A_{np}(\lambda, \Delta t) = -\log\left(\frac{I_{probe\ p}(\lambda, \Delta t)}{I_{probe\ np}(\lambda, \Delta t)}\right) \quad (1)$$

with  $I_{probe\ p}$  and  $I_{probe\ np}$  the probe intensity transmitted by the sample with and without the pump respectively. Measurements for different pump-probe delays and different wavelengths allow to reconstruct the sequence of events leading to the formation of intermediates or the photoreaction products. Unstable intermediates regardless their electronic state always have an absorption spectrum. As an example, Figure 5 below illustrates a model involving the formation of a transient non-emissive product in a singlet ground state ( $S_{prod}$ ) from  $S_1$ . In that case, the differential absorbance of the sample corresponds as:

$$\Delta A(\lambda, \Delta t) = [\varepsilon_{ESA}(\lambda) - \varepsilon_{SE}(\lambda) - \varepsilon_{GSB}(\lambda)] \times l \times c_1(t) + [\varepsilon_{product}(\lambda) - \varepsilon_{GSB}(\lambda)] \times l \times c_{product}(t) \quad (2)$$

with  $\varepsilon_{GSB}(\lambda)$ ,  $\varepsilon_{ESA}(\lambda)$  and  $\varepsilon_{product}(\lambda)$  the absorption coefficients of  $S_0$ ,  $S_1$  and  $S_{product}$  states, respectively, and  $\varepsilon_{SE}(t)$  the stimulated emission coefficient of  $S_1$ .  $c_1(t)$  and  $c_{product}(t)$  are the time-dependent concentrations of the  $S_1$  and  $S_{product}$  states and  $l$  is the probed optical path. In such a case, the  $\Delta A$  spectra are expected to display several overlapping bands reflecting contributions of the different states created by the pump:

- a negative band arising from the ground-state bleach (GSB) due to the depopulation of the ground-state induced by the pump,
- a negative band arising from the stimulated emission (SE) from the excited-state,
- a positive band arising from the excited-state absorption (ESA),
- and a positive band arising from the product ground state absorption.

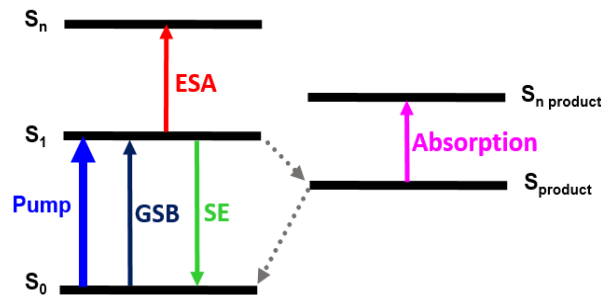


Figure 5. Three-state population model illustrating the formation of a transient non-emissive product in the singlet ground state from  $S_1$ .

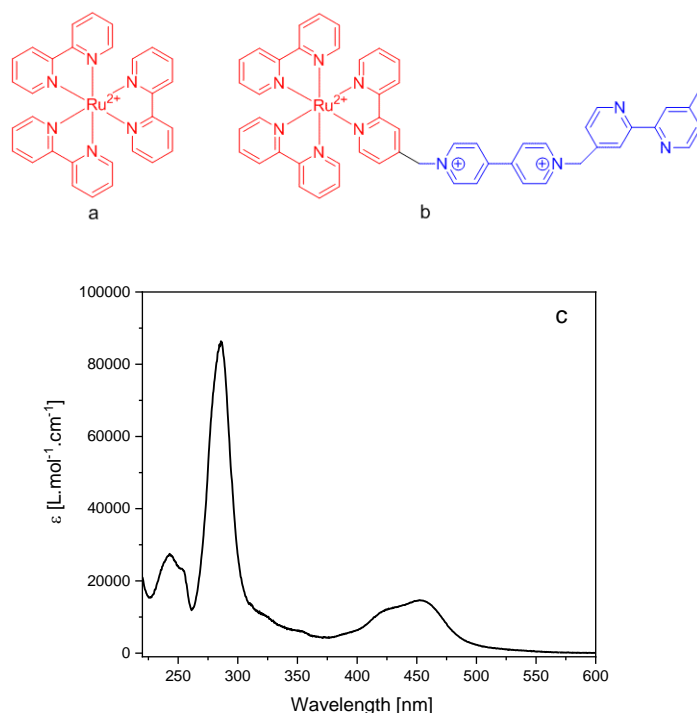
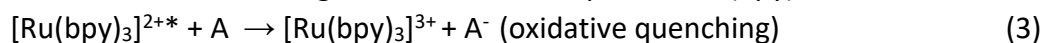


Figure 6. Molecular formulas of (a)  $[Ru(bpy)_3]^{2+}$  dye; (b)  $Ru(bpy)_3]^{2+}$ - $MV^{2+}$  dyad and (c) steady-state absorption spectra of  $[Ru(bpy)_3]^{2+}$  dye in water.

In this chapter, we focus on the use of transient absorption on time scales spanning femtoseconds to milliseconds to investigate the photophysics and the photochemistry of inorganic systems. In this regard, we have chosen to discuss two model systems based on ruthenium complexes shown in Figure 6. The first example is the prototype compound,  $[Ru(bpy)_3]^{2+}$  (bpy : 2,2'-bipyridine), which has been of the most widely studied in the last few decades (for review see [8]). The lowest singlet excited state of  $[Ru(bpy)_3]^{2+}$  pertains to a metal-to-ligand charge transfer ( $^1MLCT$ ) state, in which an electron of a metal-centered d orbital is transferred toward a  $\pi^*$  orbital of the bpy ligands. Note however that, although the localization of the transferred electron on one ligand  $\pi$  orbital in the excited state of  $[Ru(bpy)_3]^{2+}$  is generally accepted, the formation mechanism remains a matter of discussion in the literature [9]. After excitation, the initially formed  $^1MLCT$  state undergoes a fast intersystem crossing in less than 100 fs leading to the formation of the triplet state ( $^3MLCT$ ) with a quantum yield close to the unity [10-12]. While these fast events can be monitored by femtosecond transient absorption, the formed  $^3MLCT$  state whose lifetime is relatively long ( $\tau \approx 0.6 \mu s$ ) can be easily resolved by nanosecond transient absorption measurements. This relatively long-lived state has a remarkable property of being both more oxidized and reductive than the ground state. This unique combination of redox properties, excited-state lifetime and chemical stability makes this molecule play a key role in the development of inorganic photochemistry and fundamental research on photoinduced electron and energy transfer leading a wide range of applications from medicine to artificial photosynthesis or photocatalysis [13, 14]. The redox reaction of  $[Ru(bpy)_3]^{2+*}$  can give rise either to an oxidative quenching or a reductive quenching since the lowest excited state is both a good electron donor and a good electron acceptor (see eq. 3-4). Time-resolved absorption

techniques are particularly well adapted for the observation of the redox products of  $[\text{Ru}(\text{bpy})_3]^{2+*}$ . Some examples of excited-state reactions of  $[\text{Ru}(\text{bpy})_3]^{2+}$  for mechanistic studies using these techniques at different timescales will be discussed in more detail later in this chapter. The product of the oxidative quenching of  $[\text{Ru}(\text{bpy})_3]^{2+*}$  can be monitored by the loss of ground state absorption (GSB) in the 450-nm spectral region (Figure 6c), which results from the formation of the oxidized species  $[\text{Ru}(\text{bpy})_3]^{3+}$ . Reductive quenching can also be characterized by the loss of ground state absorption, in addition to the strong absorption band centered at 510 nm stemming from the reduced species,  $[\text{Ru}(\text{bpy})_3]^+$ .



The second example, we will address in this chapter, consists of the combination of  $[\text{Ru}(\text{bpy})_3]^{2+}$  and methyl viologen (N,N'-dimethyl-4,4'-bipyridine dication,  $\text{MV}^{2+}$ ) in a molecular dyad (Figure 6b).  $\text{MV}^{2+}$  has been extensively used as a reversible electron acceptor and transporter in many photochemical reactions [15-17]. In this covalently bound system, the reaction of the  $^3\text{MLCT}$  state of  $[\text{Ru}(\text{bpy})_3]^{2+}$  and  $\text{MV}^{2+}$  by oxidative quenching results from an intramolecular electron-transfer process which has been shown to be very rapid in contrast to multicomponent systems where the charge separation process is effectively limited by diffusion in solution. Therefore, while nanosecond laser flash photolysis can be used to characterize the quenching of the excited state of  $[\text{Ru}(\text{bpy})_3]^{2+}$  in a bimolecular process in solution, femtosecond pump-probe spectroscopy is needed for studying the intramolecular reaction in the dyad.

We have discussed several examples of electron transfer from the  $^3\text{MLCT}$  state of ruthenium complexes. However, it should be noted that electron transfer can also occur from the  $^1\text{MLCT}$  state in photoinduced electron injection to semiconductors [18-22]. In these cases, electron injection is a quite complex process that takes place in excited state on the timescale of hundreds of femtoseconds in competition with intersystem process. The  $^3\text{MLCT}$  state can also further contribute to the injection processes at longer timescales. Several examples of the chromophore-semiconductor interface will also be illustrated along with the development of ultrafast techniques.

In the following, we will recall some basic concepts of transient absorption, and then discuss some selected topics on the recent development of this technique and its application to inorganic systems.

## 2. Experimental techniques: basics

Depending on the configuration of the transient absorption setup, either the temporal evolution of the  $\Delta A$  signals at a fixed wavelength or the full  $\Delta A$  spectrum at a fixed time *i.e.* pump-probe delay can be measured after excitation. In both cases, a two dimensional data matrix can be collected by performing measurements for different wavelengths or different times, respectively. Those two configurations that are denoted "single-wavelength" and "broadband" transient absorption respectively, are

complementary. In general, spectral information is used to identify the various intermediates of a photoreaction while kinetics profiles allow determination of their lifetimes. The detailed principle of transient absorption measurements with femtosecond and nanosecond time resolution has been already the subject of several recent reviews [23-25]. In the following, we will briefly recall their basic principles and some of the encountered artifacts. We illustrate the use of transient absorption measurements for the characterization of the MLCT states of  $[\text{Ru}(\text{bpy})_3]^{2+}$  in solution. Over the past decades, those ruthenium complexes have become reference compounds for transient absorption spectroscopy [26].

## 2.1. Nanosecond transient absorption technique

### Basic principle :

A nanosecond pump-probe setup is nowadays a commercially available system harboring several technical options, homemade instruments are becoming rare. Detailed technical reviews can be found elsewhere [23] and only the principle as well as some recent progresses will be outlined in the following. It should be recalled that the main goal is to achieve time and spectrally resolved measurements to address fully eq. (1), minimizing photodegradation of the samples. Ultimately, the setup should thus comprise a tunable nanosecond laser as the pump light source, to selectively excite the photosensitizer to its electronic excited state, and a broad band light source, stable over the entire desired time window (up to few tens of ms) and powerful enough to gate the detection down to few nanoseconds. Detection should then make use of a streak camera to record the time and spectrally resolved data for each event. However, such equipment, albeit available, is not well adapted to the multi-timescale kinetics of the photochemical events. Thus most of the setup is either devoted to the kinetic (time trace in a given spectral range, "single wavelength" configuration) or to the spectrally resolved measurement (absorbance variation at a given time delay, "broadband" configuration). In the former case a monochromator coupled to a single channel detector is used and in the latter case a spectrograph coupled to a multi-channel detector (gated or not) is used. It should be noted that both setups can be used to reconstruct the full information by successive measurements at different wavelength or time, respectively.

In the case of a kinetic measurement, a white light source stable over hundreds of microseconds has to be used. Generally, pulsed xenon arc lamps are implemented for their ease of use and robustness. However, they intrinsically limit the overall repetition rate of the data acquisition to few hertz maximum and have the drawback of being incoherent light sources with a large divergence. Therefore, the probed volume has to be relatively large imposing high pump irradiance. Hopefully, with the progress of the LED technology, such limitations may diminish. In the past decade, the availability of new light sources such as white light supercontinuum nanosecond laser has changed the way of working. Their spatial coherence allows very small samples to be efficiently probed (below 100 microns) and their repetition rates allow experiments to be run at up to 1 kHz as in femtosecond transient absorption experiments. There an optical chopper may be used to tune the probe repetition

rate to the setup acquisition frequency. This technology is more suited to the actual approach favoring a systematic measure of the full spectral information to avoid confusion when analysing the kinetics at a single wavelength. Global fitting has thus to be performed to retrieve all contributions of the transient species in the form of decay associated or species associated spectra, as discussed in section 2.2 (subsection Data analysis).

We illustrate here, as an example, nanosecond transient absorption measurements of a water solution of  $[\text{Ru}(\text{bpy})_3]^{2+}$  obtained in our laboratories by using these two different configurations (Figure 7). The sample was excited with the third harmonic of a Nd:YAG laser at 355 nm in the first case and with the 460 nm OPO laser in the second one, both experiments lead to the observation of  $^3\text{MLCT}$  state of  $[\text{Ru}(\text{bpy})_3]^{2+}$ .

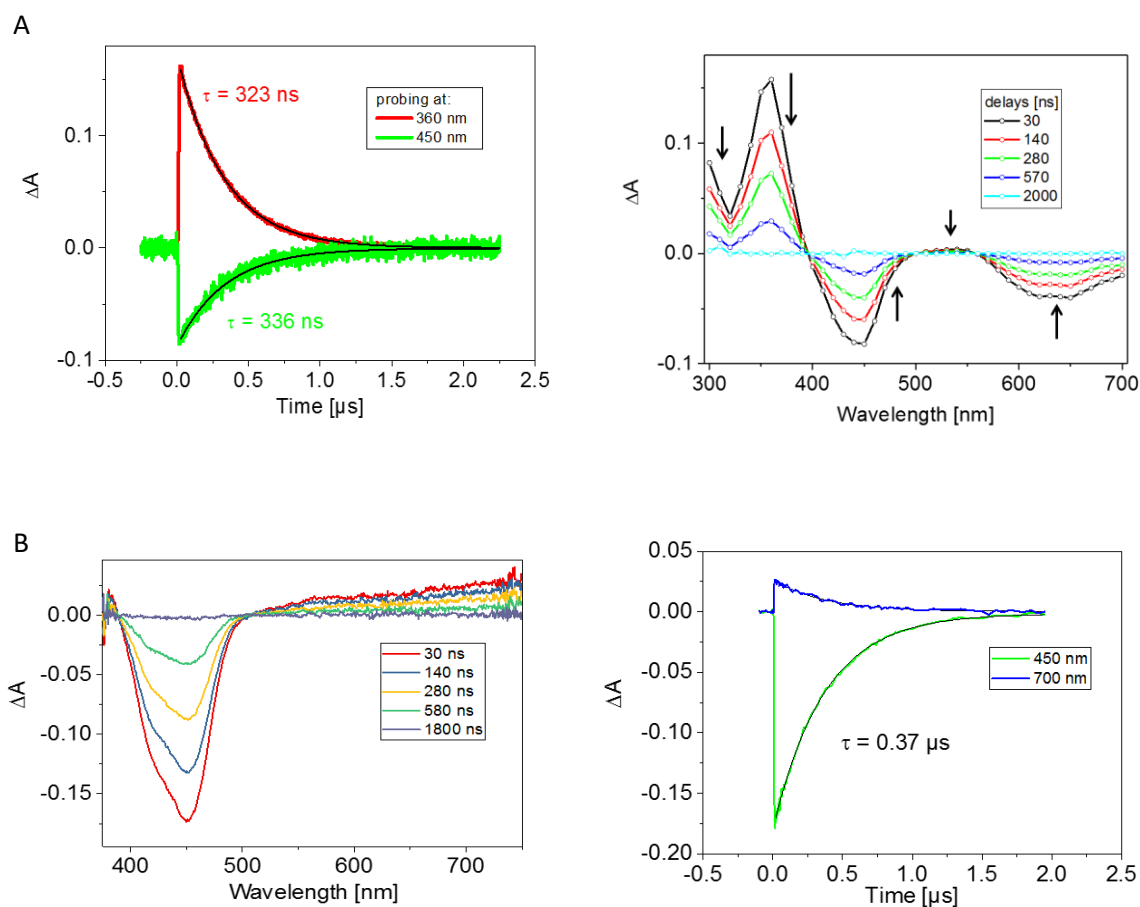


*Figure 7. Transient absorption kinetics and spectra of the triplet state of  $[\text{Ru}(\text{bpy})_3]^{2+}$  in water obtained using single wavelength measurements (A) and broadband measurements (B). In case (A) kinetics are measured in real-time by PMT coupled to a digital oscilloscope, and the transient spectra are calculated by data processing. In case (B) transient spectra at selected delay are measured by ICCD camera, and the kinetics can be calculated.*

In the first configuration, the single-wavelength  $\Delta A$  decays were measured with 10 nm steps in the wavelength range between 300 and 700 nm and the reconstructed  $\Delta A$  spectra obtained at a given delay time after the excitation are shown in the Figure 7A. The  $\Delta A$  spectra exhibit positive signals between 360–380 nm and two negative bands centered

around 450 and 620 nm, respectively. The positive absorption band in the UV region results from the dominant contribution of stronger ESA, that is attributed to the  $\pi\pi^*$  transition localized on the reduced  $\text{bpy}^-$  ligand of the  $^3\text{MLCT}$  state.[27] The negative band at 450 nm arises from the dominant contribution of the GSB (differential molar absorption coefficient  $\Delta\epsilon_{448} = -1.13 \times 10^4 \text{ M}^{-1} \text{ cm}^{-1}$ ) whereas the one at 620 nm results from spontaneous emission *i.e.* phosphorescence from the  $^3\text{MLCT}$  state. The  $\Delta A$  decays at these different wavelengths can be fitted with a mono-exponential function with a time constant of ca. 320-330 ns indicating they all result from the relaxation process of the  $^3\text{MLCT}$  excited state to the ground state.

In the second configuration, the  $\Delta A$  spectra measured in wavelength range of 380-800 nm for different time delays and the reconstructed  $\Delta A$  decays at 450 nm and 700 nm are given in Figure 7B. In this example, the negative phosphorescence band at 620 nm is no longer visible in the transient spectra since it has been suppressed by subtracting the spontaneous emission spectrum obtained from the measurements with the probe beam switched off. The positive absorption band observed at wavelengths above 500 nm is also attributed to the transition localized on the reduced ligand as observed at 380 nm. The  $\Delta A$  kinetic profiles at the 450 nm in the GBS and at 700 nm in the absorption band of the reduced ligand exhibit the same exponential decay with the time constant of  $370 \pm 5 \text{ ns}$ .

#### **Spontaneous emission correction:**

The pump pulses can induce spontaneous emission (fluorescence or phosphorescence) from the sample, which may interfere with the probe light detection. This results in the observation of strong negative signals in the  $\Delta A$  spectra as previously shown (Figure 7A). The contribution of spontaneous emission to the  $\Delta A$  spectra can be easily corrected by subtracting the measured signals without the probe beam.

#### **Polarization artifacts:**

Laser sources generally deliver linearly polarized light. When molecules are excited by linearly polarized light, only transition dipole moments oriented in a direction close to that of the pump electric field vector will absorb the light. The spatial distribution of the excited molecules is then anisotropic. If the excited molecules reorient during the lifetime of their excited state, their spatial distribution tends to become isotropic again. Typically, rotational diffusion of small molecules in fluid solvent occurs on the picosecond time scale and thus may interfere with transient absorption measurements at short time scales.

If the polarization direction of the probe is parallel to that of the pump, then the excited molecules whose transition moment is oriented in a direction close to that of the probe electric field vector will be preferentially probed. Conversely, if the polarization direction of the probe is perpendicular to that of the pump, part of the excited molecules whose transition moment is oriented in a direction close to that of the probe electric field vector will be probed. The measured differential absorbance has thus two components:

$$\Delta A(\lambda, \Delta t) = \cos^2(\theta) \times \Delta A_{//}(\lambda, \Delta t) + \sin^2(\theta) \times \Delta A_{\perp}(\lambda, \Delta t) \quad (5)$$

with  $\theta$ , the direction between the pump and probe polarization.  $\Delta A_{//}$  and  $\Delta A_{\perp}$  are the differential absorbance measured with parallel and perpendicular pump and probe polarization directions, respectively. For an isotropic population of excited molecules, the following relationship is expected:

$$\Delta A(\lambda, \Delta t) = \Delta A_{//}(\lambda, \Delta t) + 2 \times \Delta A_{\perp}(\lambda, \Delta t) \quad (6)$$

Therefore, to get rid of the anisotropic distribution of excited species created by a linearly polarized pump, the magic angle ( $\theta=54.7^\circ$ ) between the pump and probe polarization directions has to be used. Figure 8 illustrates the measurements of the  $\Delta A$  signals of  $[\text{Ru}(\text{bpy})_2(\text{dcbpy})]$  in a mixture of water and glycerol, for various orientations of the pump and probe polarization direction. Note that this asymmetric ruthenium complex is well-known to display a stronger anisotropy than the symmetric  $[\text{Ru}(\text{bpy})_3]^{2+}$  [28]. Consequently, for parallel pump-probe polarization direction ( $\theta=0^\circ$ ),  $[\text{Ru}(\text{bpy})_2(\text{dcbpy})]$  exhibits larger bleaching signals that those recorded at the magic angle ( $\theta=54.7^\circ$ ), and smaller signals for perpendicular polarization direction ( $\theta=90^\circ$ ). This difference arises from the rotational diffusion of the complex. For a sphere of radius R, the rotational diffusion time is given by:

$$\tau_{rot} = \frac{4\pi R^3 \eta}{3kT} \quad (7)$$

with k, the Boltzmann's constant, T, the temperature and  $\eta$ , the solvent viscosity.

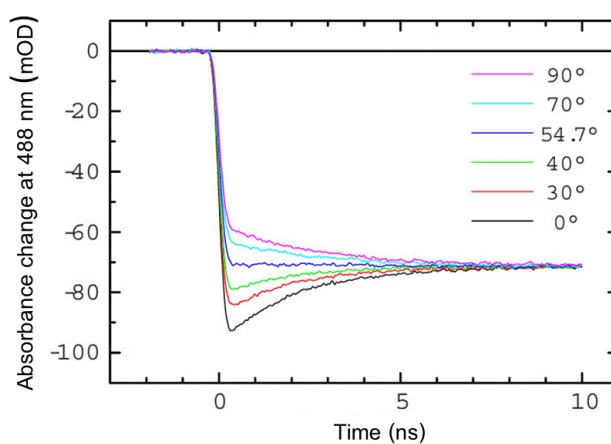


*Figure 8. Differential absorbance of  $[\text{Ru}(\text{bpy})_2(\text{dcbpy})]$  after excitation at 488 nm in 60% (w/w) glycerol/water for different angles between the polarizations of the monitoring light and the excitation pulse at 20 °C. The carboxyl-substituted ruthenium complex  $[\text{Ru}(\text{bpy})_2(\text{dcbpy})]$ , [Bis(2,2'-bipyridine) (4,4'-dicarboxy-2,2'-bipyridine) ruthenium(II) di(hexafluorophosphate)] was prepared from  $\text{Ru}(\text{bpy})_2\text{Cl}_2$  and 2,2'-bipyridine-4,4'-dicarboxylic acid. Reproduced from M. Byrdin, V. Thiagarajan, S. Villette, A. Espagne, K. Brettel, *Rev. Sci. Instrum.* 80, 043102 (2009) with the permission of AIP Publishing.*

On the other hand, time-dependent anisotropy measurements,  $r(\lambda, \Delta t)$ , can also provide important information on the rotational diffusion of chromophores or the orientation of their transition dipole moment. Anisotropy in transient absorption

measurements is however complicated to interpret due to the contribution of several transitions, such as GSB, SE and ESA.  $r(\lambda, \Delta t)$  is defined as:

$$r(\lambda, \Delta t) = \frac{\Delta A_{//}(\lambda, \Delta t) - \Delta A_{\perp}(\lambda, \Delta t)}{\Delta A_{//}(\lambda, \Delta t) + 2 \times \Delta A_{\perp}(\lambda, \Delta t)} \quad (8)$$

## 2.2. Femtosecond transient absorption technique

To study the early stages of the photoinduced processes UV-vis transient absorption with femtosecond temporal resolution can be used. This is a pump-probe technique. Nowadays, the short pump and probe pulses are typically provided by femtosecond amplified Ti:sapphire lasers delivering pulses of few millijoules in the near infra-red (750-1000 nm) at a repetition rate of a few kHz. Additional non-linear optical modules, such as optical parametric amplifiers or sum and difference frequency generator can be used in order to tune the fundamental laser wavelength over a wide spectral range going from UV to the near IR. The probe pulses can be generated by such modules for single-wavelength  $\Delta A$  measurements or by using a white light continuum generation process in the case of broadband transient absorption setups. White light continuum is generated by self-phase modulation by focusing the fundamental beam in a transparent Kerr medium such as thin plates made from  $\text{CaF}_2$ , sapphire or YAG crystal. The resulting probe pulse spectrum typically covers wavelengths from 330 nm up to 1500 nm (Figure 9). The propagation of very short laser pulses induces a change of the refractive index of the medium that produces a phase shift in the light wave leading to a change of the pulse frequency spectrum. Additional mechanism as free-electron generation in the self focus by multiphoton excitation has been also proposed.[29]

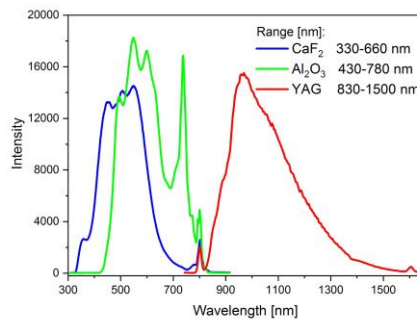


*Figure 9. White light continua obtained by focusing ~100 fs laser pulses ( $\lambda = 800$  nm) in a selection of media:  $\text{CaF}_2$ ,  $\text{Al}_2\text{O}_3$  or YAG crystal.*

### Broadband transient absorption setups:

In such setups, the probe intensity transmitted by the sample is recorded by a multichannel detector (typically CMOS or InGaAs arrays) through a polychromator. There are now detectors capable of recording every single white light continuum spectrum at a rate of 1000 spectra per second. Typically, the spectral acquisition is carried out sequentially by alternating the measurement of the probe intensity transmitted by the sample with or without the pump. Modulation of the pump at 500 Hz is performed by a mechanical chopper,

as illustrated in Figure 10. The  $\Delta A$  spectrum for a fixed pump-probe delay is then determined using equation 1.

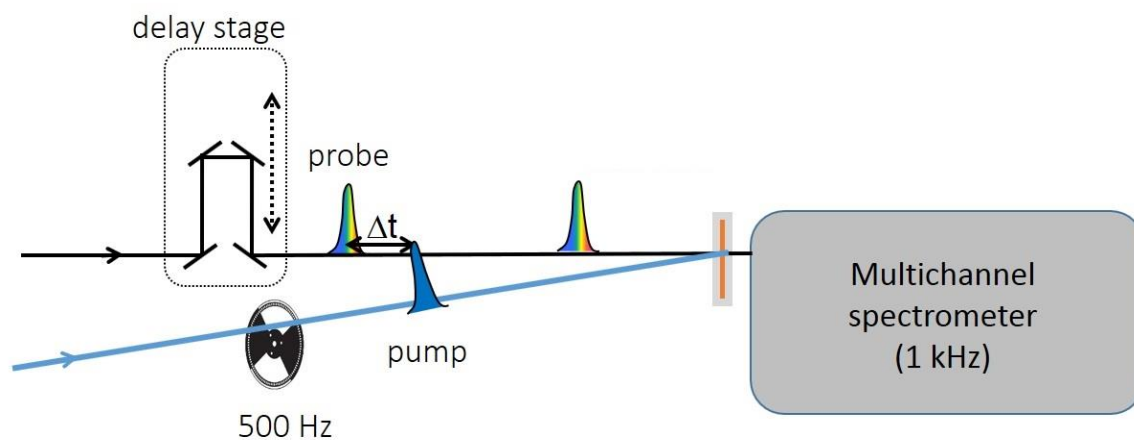


Figure 10. Simplified scheme for ultrafast UV-vis transient absorption measurements. Pump and probe originate from one amplified 1kHz femtosecond Ti:sapphire laser.

To obtain full spectral and kinetic information on the studied samples, the  $\Delta A$  spectra has to be recorded for different pump-probe delays set by an optical delay line consisting of a computer-controlled motorized translation stage mounted with a retroreflector. The typical time-window is of few nanoseconds, corresponding to a displacement of a few tens of centimeters of the retroreflector ( $\Delta t = 2d/c$ , with  $c$  the speed of light and  $d$ , the distance travelled by the retroreflector). In order to get accurate  $\Delta A$  signals, the spatial overlap between the pump and probe beams in the sample should be ensured over this large time-window. For a control experiment, a water solution of  $[\text{Ru}(\text{bpy})_3]^{2+}$  can be used. Upon excitation at 446 nm, the sample quickly (ca. 15 fs) produces the  $^3\text{MLCT}$  state with a quantum yield close to unity [12]. Consequently, the observed signals are similar to those measured with our nanosecond transient absorption setup. As shown in Figure 11A, the  $\Delta A$  spectrum 1 ns after excitation exhibits the GSB band peaking at 453 nm, the ESA band at 366 nm and 610 nm arising from a transition localized on the reduced ligand. Those spectra are expected to be constant over the time range of a few nanoseconds, as shown in Figure 11B, if pump and probe are properly aligned. If this is not the case, then the delay stage should be realigned, or the collimation of the probe beam should be improved. Note that to ensure a good spatial overlap between pump and probe, the diameter to the pump is also set slightly larger than that of the probe.

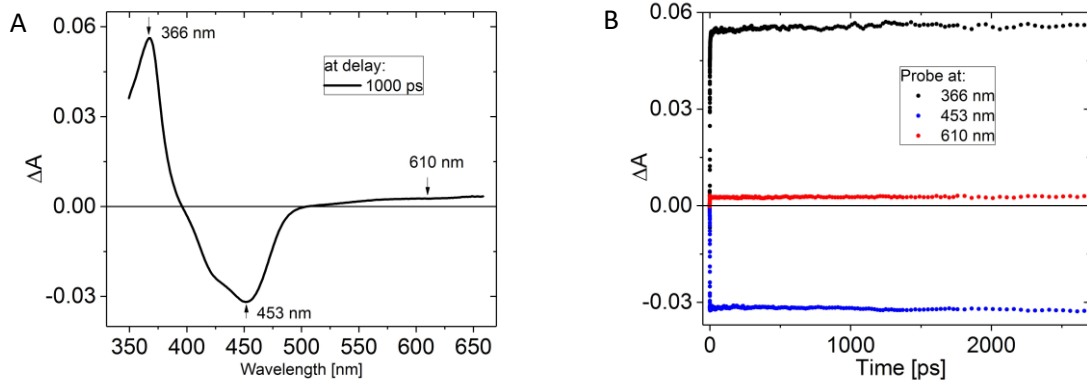


Figure 11. (A) UV-vis  $\Delta A$  spectrum recorded for a solution of  $[\text{Ru}(\text{bpy})_3]^{2+}$  in water after excitation at 446 nm. (B) Selected  $\Delta A$  kinetic traces at the probe wavelengths of 366, 453 and 610 nm.

### Signal accuracy and temporal resolution:

In order to improve the signal-to-noise ratio of broadband transient absorption measurements, it may be necessary to correct the fluctuations of the white light continuum probe. For this purpose, measurements are performed by using a double-beam detection scheme as in UV-vis steady-state spectrometers. The probe beam is divided into two beams (the probe and the reference) with a beam splitter before the sample. The probe beam is sent to the detector through the sample, while the reference beam can be directly sent to the detector. Another configuration illustrated in Figure 12 consists in sending the reference beam through the sample to the polychromator and detector. The intensity of the probe and the reference are simultaneously measured and the  $\Delta A$  signals are calculated as follow:

$$A(\lambda, \Delta t) = -\log \left( \frac{I_{\text{probe } p}(\lambda, \Delta t) / I_{\text{reference } p}(\lambda, \Delta t)}{I_{\text{probe } np}(\lambda, \Delta t) / I_{\text{reference } np}(\lambda, \Delta t)} \right) \quad (9)$$

Nowadays with fast detectors, shot-to-shot broadband detection has become possible and has been proven to significantly increase the signal-to-noise ratio of the differential spectra by eliminating most of the laser fluctuations [30].  $\Delta A$  signals with an accuracy of  $10^{-4}$ - $10^{-5}$  can be achieved [24, 31]. In order to get a good signal-to-noise ratio,  $\Delta A$  signals are averaged over a few thousands of laser shots with kHz laser sources. For some experiments, broadband detection is difficult in the middle UV (200-300 nm). In these cases, quasi monochromatic laser pulsed can be used as probe pulses. Note that single-wavelength detection setups allow measurements of  $\Delta A$  kinetics with a single laser shot and a sub-100 fs time resolution has been reported [32, 33].

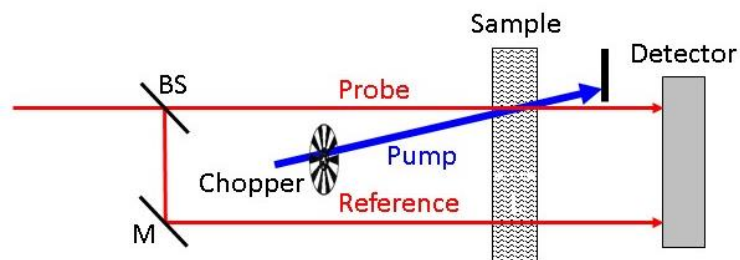


Figure 12. Simplified scheme of a femtosecond pump-probe setup using a reference probe beam for the correction of the probe intensity fluctuations. BS: 50% broadband beam splitter; M: broadband dielectric mirror.

The temporal resolution of the recorded  $\Delta A$  signals is mainly limited by the cross correlation function of the laser pump and probe beams in the sample. In addition to laser pulse duration, other factors are known to affect the temporal resolution attainable, including substantial cuvette thickness or additional optics such as lenses or filters in the beam path and the pump and probe beams angle. Studied samples are typically prepared for a 1-2 mm optical path quartz cells with an optical density of 0.5-1.0 at the excitation wavelength. For measurements requiring acquisitions over several laser shots, the sample solution has to be refreshed between each pump pulses in order to avoid photodegradation or excitation of long-lived species. These measurements can be made using a small Teflon-coated bar placed in the sample cell to agitate the solution. For less photostable solutions, a few tens of ml of sample is recirculated in a flow cell. For small sample volumes, mechanical rotation or a combination of rotation and translation can be performed on the sample cell during experiment. Note that all these last tricks apply to nanosecond configurations as well.

### Group velocity dispersion of the probe

As shown in Figure 13, broadband femtosecond  $\Delta A$  spectra can be distorted by the group velocity dispersion (GVD) of the probe (continuum) pulses. GVD reflects the dependence of group velocity of the probe wavelengths emerging in situation, when the probe pulse passes through dispersive media such as crystals, filters, the sample cell entrance window, etc. Consequently, there is a temporal spread of the supercontinuum spectral components, the "red" portion of the pulse arriving earlier in the sample than the "blue" one. In order to reduce this dispersion, reflecting optics are typically used for focusing the probe beam in the sample. Despite these efforts, the recorded  $\Delta A$  data generally show a difference in their time zero, i.e. the time at which pump and probe pulses temporally coincide in the sample due to the probe GVD as shown in Figure 13A. Therefore, GVD correction must be done in order to synchronize the time zero of all the probe wavelengths (see Figure 13B) [34-36].

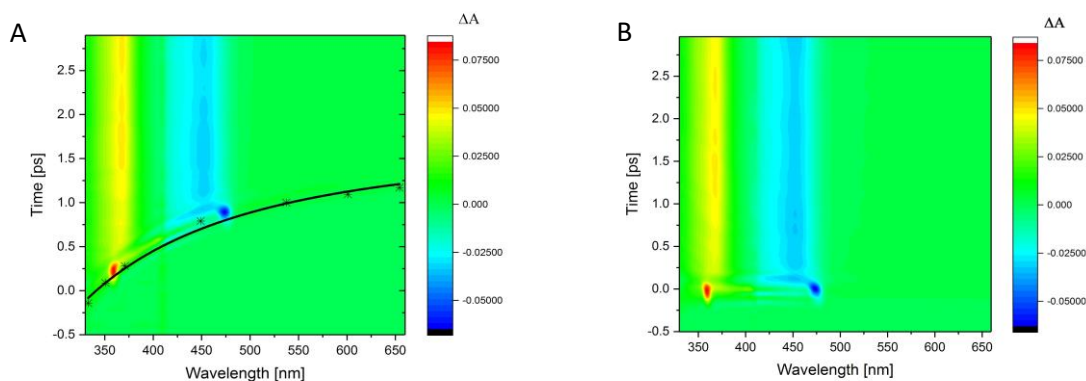


Figure 13. (A) GVD measured for a water solution of  $[Ru(bpy)_3]^{2+}$ , upon excitation at 410 nm in a 2-mm optical path sample cell. A dispersion of 1.4 ps of the time zero is observed in the 330-660 nm spectral range. (B)  $\Delta A$  spectra after GVD correction.

### Coherent artifacts

The use of ultrashort pulses can easily generate undesired non-linear effects which can distort femtosecond transient absorption signals. These artifacts arise from two-photon processes (one of the pump and one of the probe) in the sample solution or even in the sample cell and have been described in detail in [37-39]. Figure 14 illustrates three of these artifacts often encountered. Their temporal and spectral characteristics were characterized by transient absorption measurements in pure solvent. The observed signals originate from stimulated Raman scattering from the solvent, cross phase modulation of pump and probe beams (XPM) and two-photon absorption from the solvent (TPA), respectively. Stimulated Raman scattering from the solvent occurs if the difference in the energy of the pump and probe photons ( $\bar{\nu}_{pump} - \bar{\nu}_{probe}$ ) corresponds to the energy difference of two resonant vibrational states of the solvent ( $\bar{\nu}_{solvent}$ ). Figure 14A displays the coherent peaks corresponding to the stimulated Raman scattering of water pertaining to the OH vibrations at *ca.* 3400-3600  $cm^{-1}$ . The second type of artifact shown in Figure 14B corresponds to cross-phase modulation which arises from the change in the optical phase of the probe wave caused by interaction with the high energetic pump beam in the solvent. The change of the refractive index of the solvent creates a phase modulation of the probe wave leading to the observed characteristic  $\Delta A$  signal illustrated in Figure 14B. The third type of coherent artifact shown in Figure 14C is related to two-photon absorption from the solvent. Although the energy of the individual photons of the pump and probe beams cannot be absorbed by the solvent, two-photon absorption may occur if the energy density of the pump and probe pulse is high.

Coherent artifacts result from the simultaneous presence of the pump and probe pulses in the sample. Therefore, their instantaneous temporal behavior can be used to estimate the instrumental response function (IRF) and evaluate GVD effect [37, 38]. However, in some cases the presence of these artifacts can obscure the earliest steps of molecular processes. Various methods for their correction can be found in the literature [37].

Note however that the correction becomes delicate if the measured solute-related transient absorption signals are small.

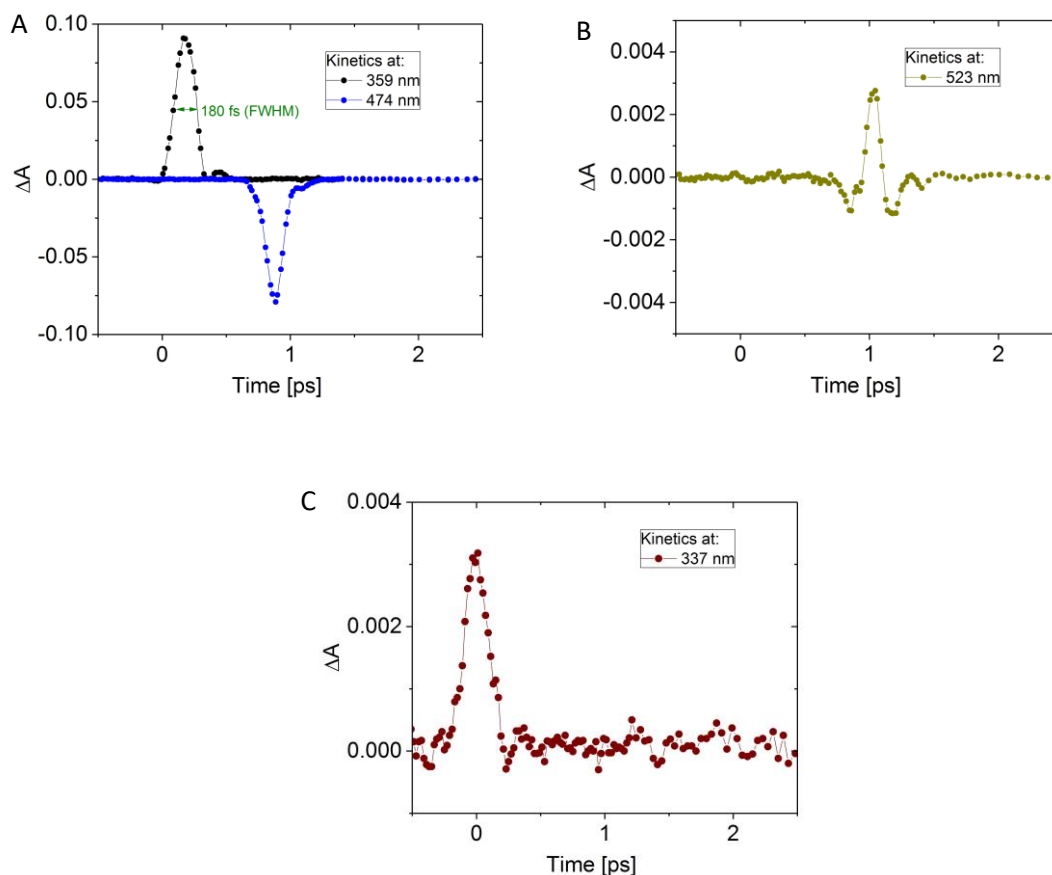


Figure 14.  $\Delta A$  kinetics traces measured in pure water. A) Stimulated Raman scattering at 359 and 474 nm due to the O-H vibrations of water upon excitation at 410 nm. The full width at half maximum (FWHM) corresponds to the IRF (180 fs). B) Cross-phase modulation of the probe at 523 nm upon excitation at 410 nm. C) Two-photon absorption signal resulting from the simultaneous absorption of pump and probe photons at 286 and 337 nm, respectively.

## Data analysis

Transient absorption measurements lead to two-dimensional data matrices depending on time and wavelength,  $\Delta A(\lambda, \tau)$ . The analysis of these matrices requires appropriate fitting procedures to extract the molecular parameters of a photoreaction. In the simplest approach, analysis of the individual kinetics at fixed wavelength can be done by using a convolution product between the IRF ( $R(t)$ ) and a sum of exponential functions:

$$F(t) = R(t) \otimes \sum_i A_i \times e^{-t/\tau_i} \quad (10)$$

with  $A_i$  the amplitude of the exponential and  $\tau_i$  the associated lifetime. Global fits of the kinetics can be also performed by using common time constants for all kinetic traces at all wavelengths. Global analysis leads to the determination of the Differential Decay Associated

Spectra,  $DADS_i(\lambda)$ , that correspond to the spectral distribution associated to each time-component,  $\tau_i$ . It is worth noting that in this approach, the absorption or emission coefficients of each contributing species are not time dependent [40, 41]. If a kinetic model is supposed instead of using a multi-exponential approach, the coupled rate equations can be used for the analysis of the experimental data. This approach is called target analysis and directly gives the Species Associated Spectra SAS( $\lambda$ ) [41]. Such an approach, which involves many more parameters than the global procedure, may not be appropriate for deciding between several kinetic models. In such cases, data analysis strategies relying on model-free methods stemming from chemometrics have been recently shown to be a powerful alternative for extracting the molecular parameters of complex photochemical processes [36].

### **3. Latest instrumental developments**

#### **3.1 Pump-pump-probe**

Pump-pump-probe spectroscopy is a valuable tool to interrogate the light-driven accumulation of electrons or holes as well as competing relaxation pathways to make multi-electron redox chemistry in artificial photosynthesis. Photoinduced electron transfer is a one electron one photon process, while photocatalytic reactions require several charge transfer events. Multiple excitation is therefore necessary to accumulate several redox equivalents to generate catalytically active sites. Using a similar principle to pump-probe absorption techniques, pump-pump-probe spectroscopy provides details on the electronic absorption behavior of a transient after a double excitation. Details on the instrument setup can be found in several recent articles focused on photoinduced charge accumulation.[42-46] We believe that this spectroscopic tool has great potential in photophysical investigation of mechanistic studies in the field of artificial photosynthesis.

Few such experiments have been reported in the literature, starting in 2010 in the group of Hammarström[42] and most recently in the group of the present authors at ISMO and in the group of Wenger in Basel.[43-46] The requirements for nanosecond pump-pump-probe experiments are multiple. Relying on the pump-probe scheme as described earlier, a nanosecond pump-pump-probe ideally uses two tunable pump lasers to select the doorway states that ignite the charge transfers. Effectively, the excited states of the different charge separated states might differ, and selective excitation could be used to optimize the first and second charge transfer. The laser beams can be counter propagating or not. The probe source is either a white light supercontinuum nanosecond laser source[43-45] for spectrally resolved measurements, or a more conventional Xenon arc lamp to access the kinetics in a given range of wavelengths.[46]

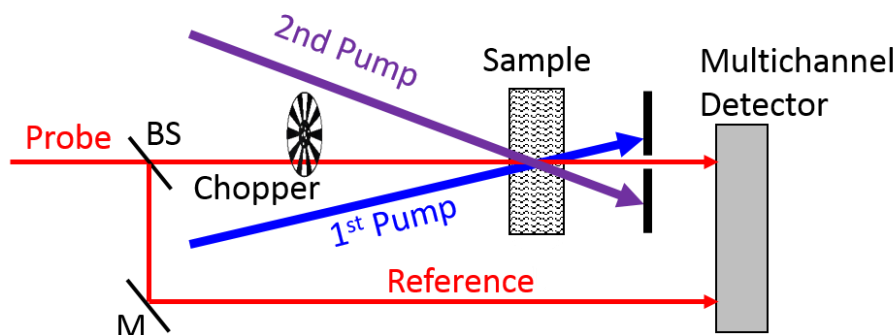


Figure 15. Scheme of the experimental setup at ISMO.[45] The two pumps are nanosecond OPO lasers that can be selectively tuned to the targeted electronic transition. The probe beam is delivered by a nanosecond white light continuum chopped at 20Hz, the duty cycle of the experiment. A reference spectrum is measured simultaneously at each event to correct the  $\Delta A$  as in eq. (9). To do so, an ICCD detector is used and two separated zone are illuminated. Note that the probe and reference laser beams are fiber-coupled for ease of alignment. BS: 50% broadband beam splitter; M: broadband dielectric mirror.

For a pump-pump-probe setup to measure variations of the optical density that are small enough ( $\Delta A \sim 10^{-3}$ ), reaching a high signal-to-noise ratio is required. Therefore a very strong requirement is the quality of the pump and probe beam spatial overlap. The two pump beams spatial profiles have to be almost the same. This can be done either by spatial filtering, which is particularly adapted for a supercontinuum laser probe with a small beam diameter and requiring low pump power [45], or by shaping the beam with beam expanders if using a (pulsed) xenon lamp. This optical beam shaping is a mandatory step to favor homogenous pumping of the solution while the probe is set at  $90^\circ$  to the optical axis of the pumps.

The three light sources have to be synchronized with the detection unit, generating two temporal delays to be controlled: that between the two pumps and that between the second pump and the probe. The chronograph has been described in detail by Mendes et al. [43] and will only be briefly explained here (Figure 15). It should be recalled that electronic control of the synchronization and delays has to be performed for nanosecond to millisecond transient absorption setups, unlike femtosecond systems where optical delay lines have to be used. The pump-pump delay has to be determined from single pump-probe measurements to optimize the population of the first charge transfer states and ensure that all transient state populations are depleted, with the remaining dynamics being only determined by the back electron transfer of the reversible triptych electron donor (or acceptor) - chromophore - catalyst. The second pump-probe delay may then be scanned to access the kinetics and/or spectrally resolved photochemistry involving the second charge separated states. There, because the efficiency of the formation of the first charge transfer is always well below 100%, a superimposition of the first (induced by pumping the remaining species in their ground state after the first pump excitation) and second charge transfer as well as all competing relaxation pathways is obtained. Deciphering all these relies on the deeply studied single pump experiment and support from spectroelectrochemistry whenever possible to identify spectral tracers of the second charge separated state [43, 45, 47, 48].

### 3.2 Basic principles of time-resolved electronic circular dichroism

Besides classical achiral pump-probe techniques, detection of chiral signals provides a powerful tool for probing conformation and dynamics of molecules in their excited state. Chirality is a geometrical property of objects, widespread in nature at various hierarchical levels. The handedness of chiral compounds can be accessed by chiroptical methods relying on the distinct interaction of dissymmetric compounds with right- and left-circularly polarized light. Notably, circular dichroism (CD) has become very popular with the advantage that the CD spectrum of complex molecular assemblies such as biomolecules can be theoretically or phenomenologically related to their conformations [49]. CD is denoted as the differential absorption of left- and right-circularly polarized light,  $A_L$  and  $A_R$  respectively:

$$CD = A_L - A_R = c l \Delta\varepsilon \quad (11)$$

with  $l$  in cm, the optical thickness of the sample,  $c$ , the concentration in mol.L<sup>-1</sup> and  $\Delta\varepsilon$  in L.mol<sup>-1</sup>.cm<sup>-1</sup> is the difference in the extinction coefficient between left- and right-circularly polarized light.

CD can be also correlated to the induced ellipticity,  $[\psi]$ , in deg.mol<sup>-1</sup>.L.cm<sup>-1</sup>, as follow:

$$[\psi] = 3298 \times \Delta\varepsilon \quad (12)$$

This property stems from the fact that linearly polarized light can be considered as an equal combination of left and right circularly polarized light. Therefore, when linearly polarized light goes through a chiral sample, the polarization of the transmitted beam becomes elliptic. Although ellipticity measurements appeared first, at the beginning of the twentieth century, the principle behind modern commercial CD spectrometers relies on the direct measurement of the differential absorbance measurements, which is less prone to artifacts [50, 51].

In time-resolved mode, circular dichroism (TR-CD) can provide useful information both about the electronic and molecular structure of chiral compounds in their excited state that is inaccessible to achiral spectroscopy [52]. However, the implementation of TR-CD to pump-probe setups remains challenging due to the very weak signals ( $\Delta\varepsilon/\varepsilon=10^{-3}$ - $10^{-6}$ ). Recent developments in pulsed laser sources as well as in polarization optics have made it possible to probe TR-CD signals over large time scales, ranging from milliseconds down to a few hundred femtoseconds, in the UV-visible domain [50, 53-63]. In a similar way as steady-state CD, the principle of all these experiments is based either on the direct measurement of the differential absorbance between left and right-circularly polarized probe after excitation [50, 55, 57, 62-64], or by the measurement of the pump-induced ellipticity on a linearly-polarized probe [51, 56, 58, 59], as illustrated in Figure 16. In addition to the artifacts generally encountered in transient absorption measurements, TR-CD measurements are very sensitive to polarization artifacts such as the birefringence of the sample cell or asymmetry in the circular polarization of the probe. Discussion of those artifacts being out of the scope of the present chapter, their details can be found in reviews devoted to TR-CD spectroscopy [50, 65, 66].

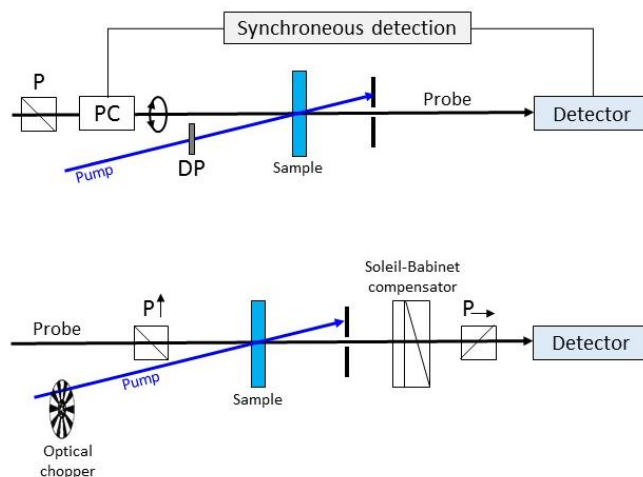


Figure 16. Basic principle of one-wavelength TR-ECD: (Up) Differential absorbance TR-ECD: the modulation of the probe polarization is performed by a photoelastic modulator (PEM) or a Pockels cell (PC). In order to avoid artifact arising from pump-induced birefringence in the sample (i.e. anisotropy), a depolarizer (DP) is inserted on the pump beam trajectory. (Down) Ellipsometric TR-ECD: the sample is placed between two crossed polarizers (P). The ellipticity of the probe beam is then measured with a Soleil-Babinet compensator or a  $\lambda/4$  waveplate inserted behind the sample cell and the two polarizers.

### 3.3 Transient absorption spectroelectrochemistry

Transient absorption can be combined with electrochemistry in order to have insights on photoinduced excited-state processes of a species being oxidized or reduced. This coupling of the spectroscopic and electrochemical techniques is referred as transient absorption spectroelectrochemistry (TA-SEC).

In general, spectroelectrochemical measurements are made in a cell containing three electrodes: working, reference and counter electrodes. These electrodes need to be arranged to have transparency in UV-Vis light for transmission measurements. For the majority of reported experiments, the use of optically transparent electrodes (OTE) is required for the measurements in transmittance mode [67-69]. Different electrode materials have been considered: thin conducting film electrodes made of a thin layer of metal deposited on an optically transparent substrate or minigrad electrodes made of a non-transparent metal such as gold or platinum. A slit or a hole can be designed in the working electrode to allow the pump and the probe beams to pass through the cell.  $\text{Ag}/\text{Ag}^+$  in a miniaturized version and Pt wire are often used as the reference and counter electrode, respectively. Of note, electrolysis of a large volume of solution can be relatively slow. Optically transparent thin layer electrodes (OTTLE) are thus widely used for the fast electrolysis of all the species in the light path. An example of configuration for TA-SEC measurements is illustrated in Figure 17. Transient absorption experiments of electrochemically oxidized or reduced compounds are carried out after exhaustive electrolysis at appropriate potentials. Solutions need to be maintained under an inert atmosphere of argon or nitrogen during all experiments. In order to decrease degradation or local heating effects, the cell can be moved during the measurements.

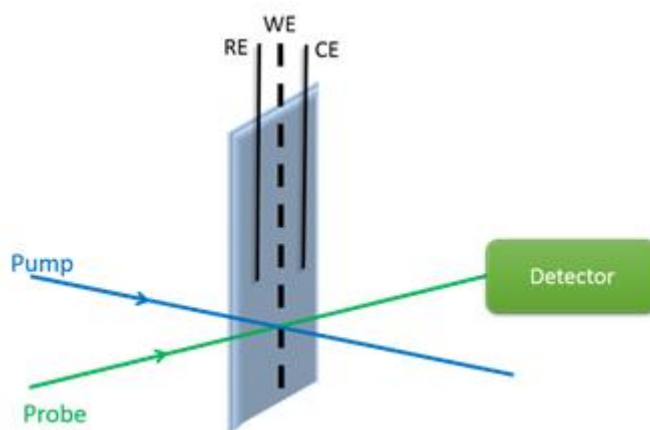


Figure 17. Electrochemical cell for transient absorption spectroelectrochemistry measurements.

## 4. Applications

### 4.1. Pump-probe experiments

One of the most studied photochemical reactions in transient absorption is the photoinduced electron transfer. As example, let us consider electron transfer reactions between  $[\text{Ru}(\text{bpy})_3]^{2+}$  and methyl viologen ( $\text{MV}^{2+}$ ), which has been extensively used as a reversible electron acceptor and transporter in many photochemical reactions. Depending on the molecular structure, the electron transfer rate can vary from microsecond to femtosecond timescales.

Time-resolved spectra investigated by nanosecond transient absorption of a  $[\text{Ru}(\text{bpy})_3]^{2+}$  and  $\text{MV}^{2+}$  mixture are shown in Figure 18. Photoexcitation of the ruthenium chromophore populates the  $^3\text{MLCT}$  excited state, which undergoes a charge transfer to the  $\text{MV}^{2+}$  acceptor. The excitation results in an almost instant formation of the bleaching band at 460 nm corresponding to disappearance of the ground state absorption of  $[\text{Ru}(\text{bpy})_3]^{2+}$ . Formation of new absorption features are observed as an increase in absorption of the bands centered at 390 and 600 nm with a rate constant of  $90 \pm 10$  ns. These bands are assigned to the formation of reduced methyl viologen, which is formed following oxidative electron transfer from the excited ruthenium complex to  $\text{MV}^{2+}$ . On a longer time scale, the decrease of transient absorption bands of the reduced methyl viologen is accompanied by a diminution of the bleaching band of the ruthenium complex due to the charge recombination process occurring with a second-order rate constant.

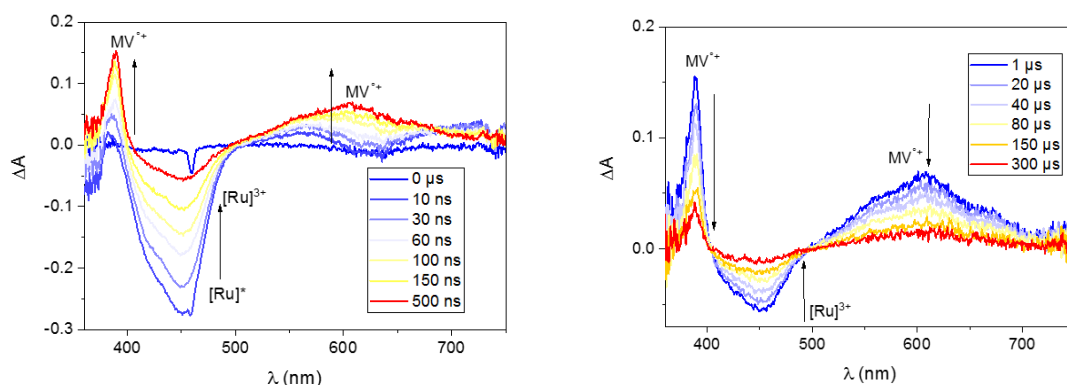


Figure 18. Transient spectra at indicated delay times generated by 460 nm laser excitation of  $[\text{Ru}(\text{bpy})_3]^{2+}$  ( $35 \mu\text{M}$ ) and  $\text{MV}^{2+}$  ( $10 \text{ mM}$ ) in Ar-saturated water.

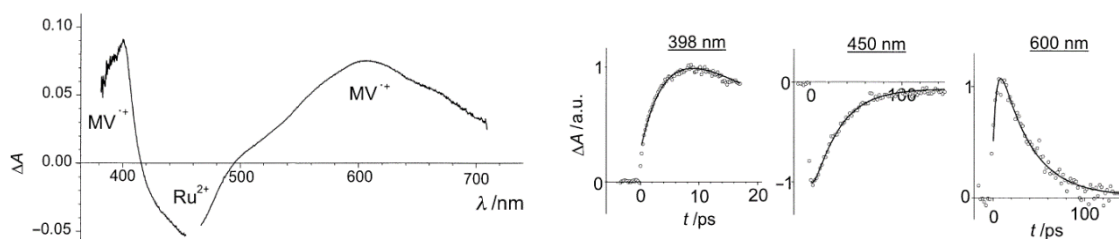
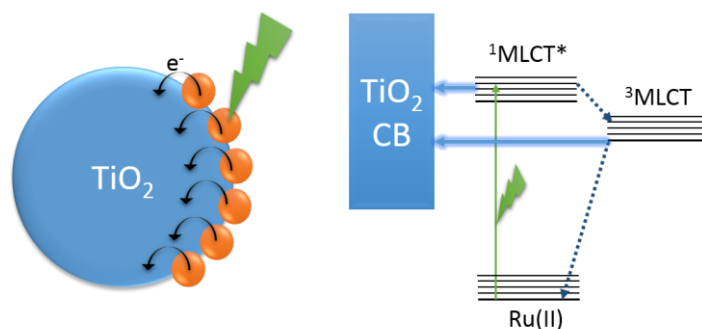


Figure 19. Transient spectra at 10 ps and kinetic traces at indicated wavelength produced by 460 nm laser excitation of  $[\text{Ru}(\text{bpy})_3\text{-MV}]^{4+}$  dyad in acetonitrile. Reproduced from Ref. [68] with permission from John Wiley and Sons.

In contrast to multicomponent systems, the charge separation processes in covalently linked systems occurs much more rapidly since it is not limited by diffusion. The second example here illustrates the ultrafast electron transfer of the same molecular species covalently bound in a molecular dyad (Figure 19) investigated by femtosecond pump-probe spectroscopy. The transient spectrum at 10 ps clearly indicates the formation of a charge separated state, with the photobleaching band of ruthenium at 450 nm and the positive absorption bands of  $\text{MV}^{+•}$  at 398 and 600 nm by oxidative quenching of the  $^3\text{MLCT}$  state of  $[\text{Ru}(\text{bpy})_3]^{2+}$ . The kinetic traces at these wavelengths were fitted with the same time constants corresponding to the charge separation ( $\tau_{\text{CS}} = 4.5 \pm 0.5 \text{ ps}$ ) and the charge recombination ( $\tau_{\text{CS}} = 30 \pm 2 \text{ ps}$ ).



*Figure 20. Illustration of excitation of Ru(II)-polypyridyl dye sensitized TiO<sub>2</sub> and electron injection to the CB of TiO<sub>2</sub> following MLCT excitation of Ru(II) chromophore.*

Taking advantage of ultrafast transient absorption technique, photoinduced electron transfer in transition metal complexes sensitizing nanostructured semiconductors has been extensively studied in the context of solar energy conversion [18, 21, 22, 70]. The understanding of the dynamics of electron transfer in these hybrid assemblies can be seen as a stepping stone towards the development of efficient solar cell devices. Ru(II)-polypyridyl chromophores absorbed on nanostructured titanium dioxide have been widely used as model systems for the studies of ultrafast interfacial photoinduced electron transfer. Upon visible absorption of Ruthenium chromophores anchored to the surface, the excited molecules can inject electrons into the TiO<sub>2</sub> conduction band (Figure 20). Femtosecond pump-probe spectroscopy allows measurements of the charge injection kinetics by following either the excited or the oxidized states of the chromophore. The electron injection kinetics depend on the nature of the chromophore and the semiconductor as well as the measurement conditions but most of studies showed a very fast and complex process with nonexponential kinetic behaviors. A typical study of the interfacial charge transfer in the Ru(dcbpy)<sub>2</sub>(NCS)<sub>2</sub> (RuN3; dcbpy = 4,4'-dicarboxy-2,2'-bipyridine) sensitized TiO<sub>2</sub> film has been reported by Benkő and coworkers [19]. An ultrafast time constant of 30 fs is attributed to the formation of oxidized product resulted from a rapid electron injection from the singlet excited <sup>1</sup>MLCT in competition with intersystem crossing to the <sup>3</sup>MLCT state. Furthermore, it was demonstrated that further electron injection from the <sup>3</sup>MLCT state with a multiexponential kinetic occurs within the 1-50 ps time scale. An example of the transient spectra of this assembly at different time delays is shown in Figure 21. At picosecond time scale, the decay of triplet excited state at 690 nm and 1050 nm can be correlated to the rise of the oxidized state of the chromophore at 860 nm, indicating the electron injection from the triplet state to TiO<sub>2</sub>. These results led the authors to the conclusion of the different mechanisms of photoinduced charge injection in the interface which is triggered from both initially populated singlet state and the excited triplet state of the chromophore. (Figure 20)

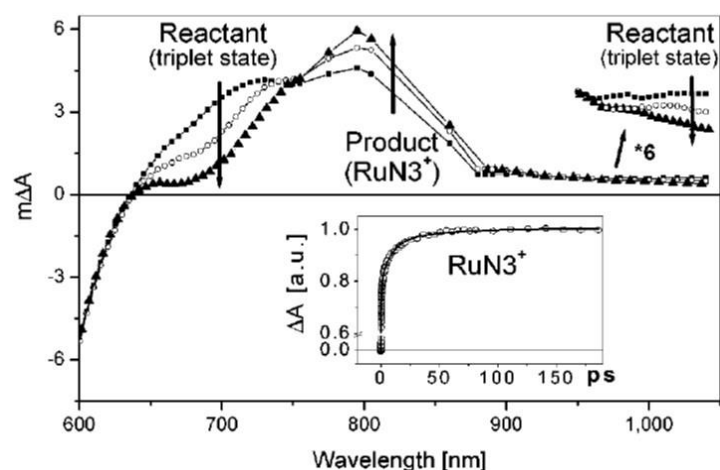


Figure 21. Transient absorption spectra observed by 530 nm laser excitation of RuN3-sensitized TiO<sub>2</sub> film at time delay of 0.5 (■), 10 (○) and 150 ps (▲) pump-probe delay. Inset: Time profile at 860 nm corresponding to RuN3 cation. The figure was published in Ref. [19] and reproduced by permission of the American Chemical Society.

#### 4.2. Multiple-charge photo-accumulation by pump-pump-probe experiments:

Light-driven single electron transfer processes stand as the basis for the majority of reported photocatalytic processes. However, catalytic solar fuel formation reactions are evidently multielectronic transformation and require the accumulation of multiple redox equivalents at the catalytic sites where bonds are broken or formed. Therefore, a photocatalytic system has to be able to transiently accumulate several redox equivalents upon sequential absorption of several photons to complete the catalytic reactions. Pump-pump-probe experiments are necessary to study these processes and get useful information on accumulative charge separation as well as on deleterious pathways taking place after the second excitation. Examples of such experiments are however rare in the literature, only few systems were reported for the photodriven charge accumulation in a reversible fashion [71]. Among these, only several molecular covalently linked systems are able to exhibit photo-accumulation of charges without sacrificial reagents with a lifetime of charge-accumulated state superior to 1 μs. The first example is an oligotriarylamine (OTA)-Ru<sup>II</sup>-TiO<sub>2</sub> molecular/semiconductor hybrid triad system developed by the Hammarström group (Figure 22) [42]. Using ultrafast transient absorption, the excited Ru<sup>II</sup> chromophore was shown to rapidly inject electrons into the mesoporous TiO<sub>2</sub> film within 5 ps to generate OTA-Ru<sup>III</sup>-TiO<sub>2</sub><sup>-</sup> which is characterized by bleached region at 400-500 nm. The oxidized Ru<sup>III</sup> further produced OTA<sup>+</sup> by a hole transfer to the OTA donor, resulting in the growth of OTA<sup>+</sup> absorption band concomitant with Ru<sup>II</sup> ground-state recovery on a longer time scale. Pump-pump-probe nanosecond experiments were then conducted to investigate further charge separation. Figure 22 (right) shows the time-resolved spectra of the dyad measured directly after excitation. Upon single pulse excitation, about 30% of the first charge separated state (CSS1) OTA<sup>+</sup>-Ru<sup>II</sup>-TiO<sub>2</sub><sup>-</sup> was formed. The obtained transient spectrum (black curve) corresponds well with the signature of OTA<sup>+</sup> obtained by spectroelectrochemistry. When a second pulse laser was applied to reexcite the regenerated Ru<sup>II</sup> chromophore of CSS1, similar

processes were responsible for the generation of the second charge separated state (CSS2)  $\text{OTA}^{2+}\text{-Ru}^{\text{II}}\text{-TiO}_2^{2-}$  with the characteristic absorption features of  $\text{OTA}^{2+}$ . As shown in the Figure 22, the orange curve obtained by the subtraction of  $\text{OTA}^+$  signature from the green spectrum after double pulse experiment agrees well with the differential spectrum of  $\text{OTA}^{2+}$  observed upon electrolysis.

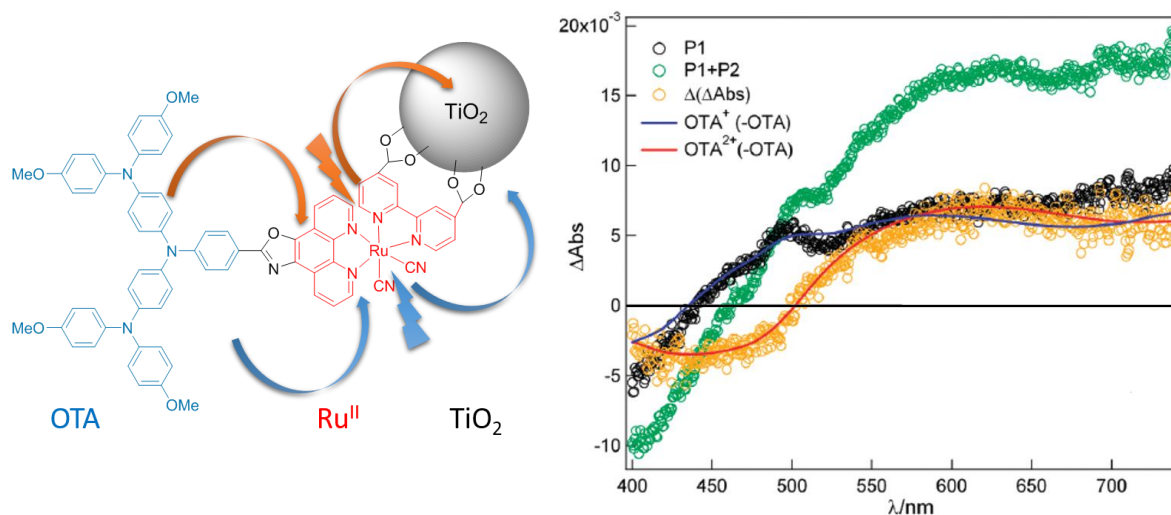


Figure 22. Structure of  $\text{OTA-Ru}^{\text{II}}\text{-TiO}_2$  and transient absorption spectra measured directly after single pulse (P1) and double pulse (P1+P2) 480 nm excitation. The orange curve indicates the difference spectrum between the double pulse and single pulse spectra. The blue and the red curves represent the differential spectra of  $\text{OTA}^+$  and  $\text{OTA}^{2+}$  obtained from spectroelectrochemistry. Reproduced from Ref. [42] by permission of American Chemical Society.

Accumulated charge separation has also been explored in molecular dyad or multicomponent systems, following two excitation events by using nanosecond pump-pump-probe experiments (Figure 23). In a molecular system consisting of a dyad holding only one photosensitizer ( $[\text{Ru}(\text{bpy})_3]^{2+}$ ) and one two-electron acceptor (naphthalene diimide NDI) in presence of a reversible electron donor, two electrons have been accumulated on the acceptor site. To investigate the second electron transfer process, a second nanosecond pulse was applied 1  $\mu\text{s}$  after the first one, when the first charge separated state is completely achieved and the sensitizer is regenerated. Compared to the single excitation, the transient absorption spectrum obtained upon double-pulse contains distinctive new features which are in excellent agreement with the reference spectrum of the doubly reduced state  $\text{NDI}^{2-}$ .

This charge accumulated state persists with a lifetime of 0.2 ms with an embarked energy of 1.1 eV above the ground state.

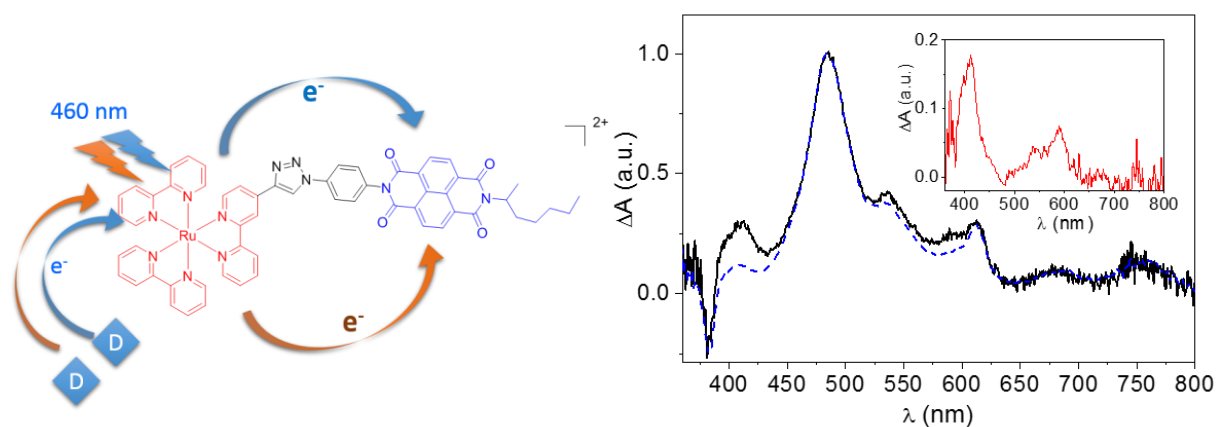


Figure 23. Molecular structure of  $[\text{Ru}(\text{bpy})_3]^{2+}$ -NDI dyad (left) and transient absorption spectra of the dyad in the presence of ascorbate, acting as an external electron donor, at 30  $\mu\text{s}$  after single pulse excitation (blue dash curve) and double pulse excitation (black solid curve). Inset shows the difference spectrum between the single and double pulse excitation which agrees well with the absorption spectrum of  $\text{NDI}^{2-}$  obtained by spectroelectrochemistry. Reproduced from Ref. [43] by permission of John Wiley and Sons.

In a different configuration, the same authors reported a complete multicomponent molecular system containing  $[\text{Ru}(\text{bpy})_3]^{2+}$ ,  $\text{MV}^{2+}$  as a two-electron acceptor and ascorbate as reversible electron donor. The transient absorption curves are presented in the Figure 24A. Upon single pulse excitation of the  $\text{Ru}^{\text{II}}$  chromophore, positive absorption bands at about 395 and 605 nm correspond to the first reduced state  $\text{MV}^{\cdot+}$ . By using the double-pulse excitation, an increase in the band at 395 nm indicates the formation of the doubly reduced methylviologen ( $\text{MV}^0$ ) species. The inset shows the difference of the two transient spectra which agrees well with the absorption spectrum of  $\text{MV}^0$  by spectroelectrochemistry. Corrected kinetic trace after the extraction of the  $\text{MV}^0$  contribution is presented in Figure 24B indicating a rise time of 12  $\mu\text{s}$  and a decay time of 50  $\mu\text{s}$ . The fraction of  $\text{MV}^0$  species detected after the second laser pulse was approximately 9%, which is comparable with intramolecular systems. This study stands as the first example where two sequential charge accumulation was evidenced in a multicomponent system in a reversible manner. Nanosecond pump-pump-probe experiments have demonstrated the possibility to drive charge accumulation in different molecular configuration, either in multicomponent or intramolecular system where the photosensitizer is covalently linked to electron acceptors and donors. The molecular systems studied in all these examples have the advantage of being very well defined species with distinguishable absorption features for different oxidation states facilitating the identification of the different products upon subsequent electron accumulation using transient absorption spectroscopy. Further development of transient spectroscopic techniques using Raman or mid IR probes should also be explored to bring complementary information on molecular structure of these active states, especially

when UV-VIS transient absorption is limited by similar absorption features of different charge separated states hampering their selective observation.

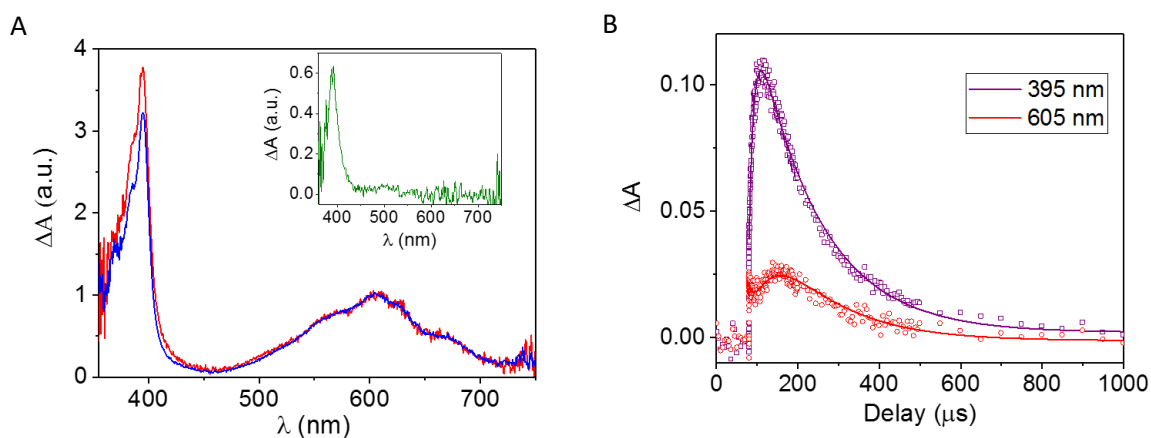


Figure 24. A) Transient absorption spectra normalized at 605 nm of  $[Ru(bpy)_3]^{2+}$  ( $43\mu M$ ) in deaerated  $CH_3CN/H_2O$  (60:40) in the presence of  $MV^{2+}$  ( $13\mu M$ ) and ascorbate ( $100mM$ ) after single pulse (blue line) and double pulse excitation (red line). Inset: difference between single and double pulse excitations at 460 nm. B) Corrected transient kinetic of  $MV^0$  at 395nm after a double-pulse excitation. Reproduced from Ref. [45] by permission of American Chemical Society.

### 4.3. Combination of transient absorption and electrochemistry

As described in the previous section, two successive photoinduced electron transfers using pump-pump-probe techniques are used to generate charge accumulative active species. An alternative experimental technique is to combine transient absorption and electrochemistry in transient absorption spectroelectrochemistry. To do this, the generation of the first reductive or oxidative species by the first pump excitation is replaced by electrolysis. The different oxidation state of methylviologen (+I,0) in the  $[Ru(bpy)_3]^{2+}-MV^{n+}$  molecular dyad was prepared by applying different potentials [68]. Using the initial oxidation state,  $MV^{2+}$ , an oxidative quenching resulting from an electron transfer from Ru to  $MV^{2+}$  was observed upon excitation of the ruthenium chromophore. However, oxidative quenching is changed to reductive quenching when  $[Ru(bpy)_3]^{2+}-MV^+$  or  $[Ru(bpy)_3]^{2+}-MV^0$  generated by electrolysis were studied. Figure 25 shows the differential absorption spectra obtained after excitation of the Ru chromophore at 460 nm. Indeed, a rapid reverse electron transfer from  $MV^+$  to  $[Ru(bpy)_3]^{2+}$  is evidenced by the formation of  $[Ru(bpy)_3]^+$  with a positive absorption at 500 nm accompanied by the bleaching of  $MV^+$  with negative absorption at about 400 and 600 nm. Similarly, reductive quenching of the chromophore of  $[Ru(bpy)_3]^{2+}-MV^0$  dyad to form  $[Ru(bpy)_3]^+-MV^+$  was also observed as shown in Figure 25. The absorption band at around 600 nm is a characteristic absorption of  $MV^+$  band, and the one at 500 nm is attributed to the absorption of the reduced chromophore  $[Ru(bpy)_3]^+$ .

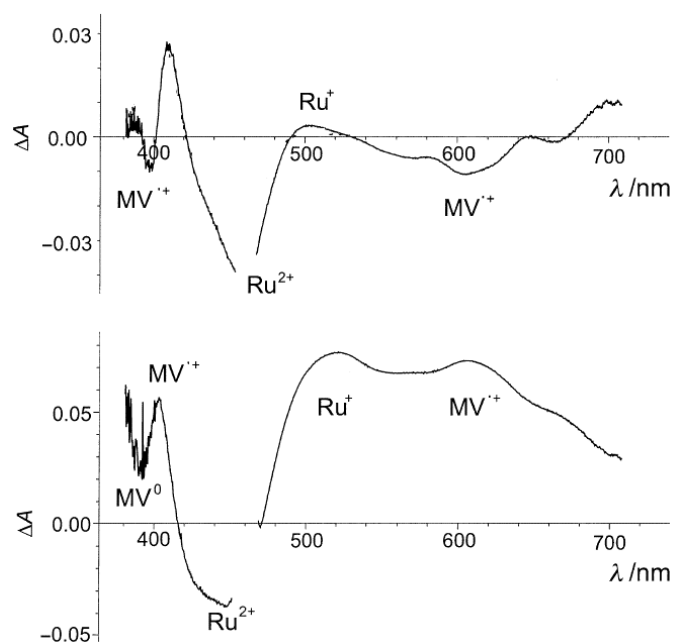


Figure 25. Transient spectra of  $[Ru(bpy)_3]^{2+}$ - $MV^+$  at 3 ps (top) and  $[Ru(bpy)_3]^{2+}$ - $MV^0$  at 5 ps (bottom) after 460 nm laser excitation. Reproduced from Ref. [68] by permission of John Wiley and Sons.

The second example of electron transfer study in a dye-cobalt catalyst assembly was recently reported using ultrafast transient absorption spectroelectrochemistry to investigate the mechanism of the cobalt catalyst activation [69]. The molecular structure of the dyad is presented in Figure 26. In the ground state, the cobalt center is in the  $Co^{III}$  state whereas the catalytically active unit is  $Co^I$ . To investigate the mechanism of the catalytic activation, the authors prepared the cobalt catalytic unit at different oxidation state (I, II) using electrochemistry. Ultrafast transient absorption was then employed to study the dyad at different oxidation states of the catalytic unit. Unfortunately, similar deactivation processes and transient signatures were obtained with all oxidation states when exciting the chromophore. The authors concluded that the activation of the catalyst should require first the reductive quenching of the chromophore by a sacrificial agent before the reduction of the catalyst.

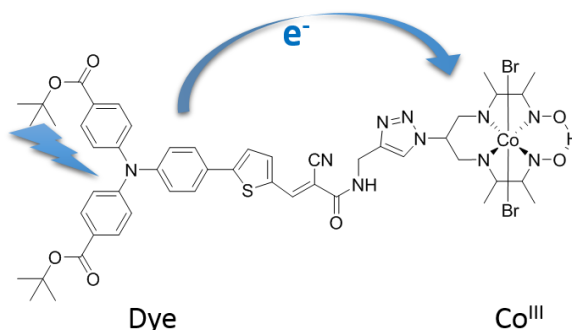


Figure 26. Structure of a dye-cobalt catalyst studied by transient absorption spectroelectrochemistry [69].

Despite the fact that these studies do not show good results on charge accumulation, this technique still remains a very interesting alternative to investigate multiple electron

transfer, an essential step for the understanding and the optimization of molecular systems for photocatalysis.

#### 4.4. Ruthenium complexes as chiral paradigms for TR-CD spectroscopy

Over the last decades, ruthenium complexes such as  $[\text{Ru}(\text{bpy})_3]^{2+}$  and  $[\text{Ru}(\text{phen})_3]^{2+}$  have become prototype chiral compounds for TR-CD studies. Due to the propeller-twist arrangement of their three ligands, ruthenium complexes, such as  $[\text{Ru}(\text{phen})_3]^{2+}$  and  $[\text{Ru}(\text{bpy})_3]^{2+}$  are chiral compounds that display very strong CD signals in the middle UV (200–300 nm) illustrated in Figure 27. Those bisignate structures are known to arise from the excitonic coupling of the three degenerated  $\pi\pi^*$  transitions of the ligands that can be used to determine their absolute configuration in the ground state [72]. They also provide a sensitive probe of the electronic structure of their three ligands after excitation [63, 64, 73, 74].

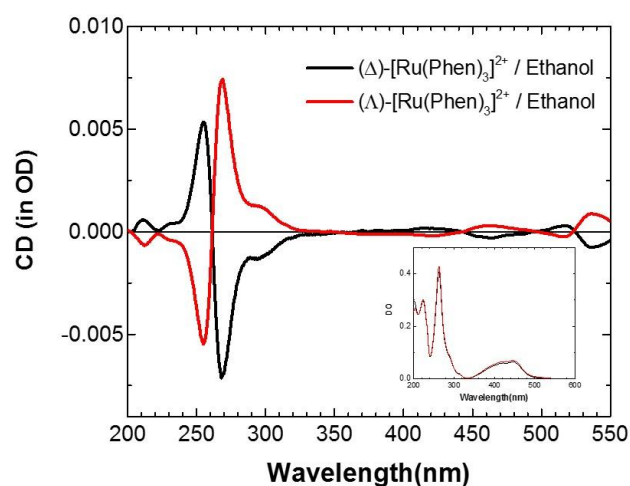


Figure 27. CD spectra of the two enantiomers of  $[\text{Ru}(\text{phen})_3]^{2+}$  measured in ethanol with a home-made spectropolarimeter in our laboratories. Insert: Corresponding absorption spectra.

Femtosecond transient absorption studies showed that, upon visible excitation,  $[\text{Ru}(\text{bpy})_3]^{2+}$  undergoes an ultrafast electron transfer from the central metal to the three ligands followed by a charge localization onto one ligand in less than 15 fs [75]. The fast intersystem crossing from the  $^1\text{MLCT}$  excited state to the long-lived  $^3\text{MLCT}$  state then takes place in ca. 300 fs [10, 12]. Figure 28 illustrates typical transient absorption and CD spectra of  $(\Lambda)\text{-}[\text{Ru}(\text{phen})_3]^{2+}$  in acetonitrile measured in the deep UV, 50 ps after excitation at 400 nm, by ellipsometric TR-CD. The  $\Delta A$  spectrum is dominated by the ground-state bleach that peaks at 260 nm and pertains to the three degenerated  $\pi\pi^*$  transitions of the ligands. The two small positive bands on both sides of the ground-state bleach have been attributed to the  $^3\text{MLCT}$  state absorption which is composed of the blue-shifted absorption band of the reduced ligand at around 240 nm and the charge transfer transition from the reduced ligand to the metal (LMCT) at around 280 nm [74, 76].

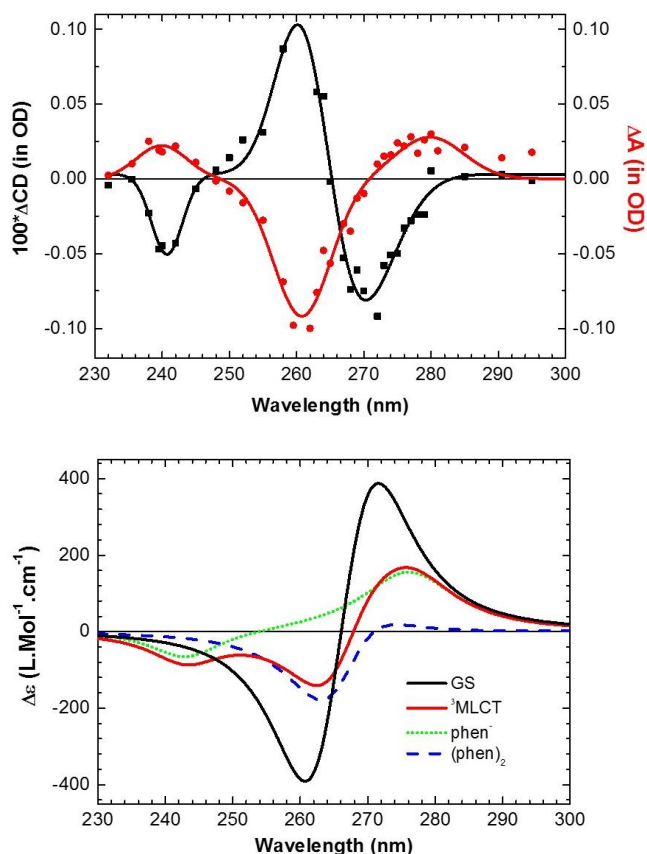


Figure 28. (Up) Transient absorption ( $\Delta A$ ) and transient CD ( $\Delta CD$ ) spectra of  $(\Lambda)$ - $[Ru(phen)_3]^{2+}$  in acetonitrile measured 50 ps after excitation at 400 nm. Signals were fitted with a sum of three Gaussian functions. (Down) Calculated CD spectra of  $(\Lambda)$ - $[Ru(phen)_3]^{2+}$  in acetonitrile: (Black line) the ground-state, (red line)  $^3MLCT$  excited state which can be decomposed into the contribution of the CD signal of the unperturbed ligands (blue dashed line) and the contribution of the reduced ligand (green dotted line). Adapted with permission from the Ref. [74]. Copyright 2007 American Chemical Society.

The transient CD spectrum of  $(\Lambda)$ - $[Ru(phen)_3]^{2+}$  is also dominated by the contribution of the ground-state CD bleach that peaks at 260 nm and 270 nm. One also observes an additional negative CD band at 240 nm which has been attributed to the excited  $^3MLCT$  state. As shown in Figure 28, calculations based on an coupled oscillator model provide clear evidence that this CD signal contains both the signature of the reduced ligand and the two unperturbed ligands [74, 77].

Through the development of very stable ultrafast laser sources, implementation of TR-CD spectroscopy on pump-probe setups now offers the opportunity to measure the changes of the electronic distribution and conformation of chiral compounds over an extended timescale, spanning a few hundred femtoseconds up to milliseconds. While the full potential of ultrafast TR-CD still remains to be explored, both theoretical and experimental studies provided evidence of the ability of such experiments to follow complex population transfers following excitation that are inaccessible to achiral measurements [52, 78, 79]. In addition, although TR-CD cannot provide an atomistic description of the sample conformation unlike time-resolved crystallography, it provides convenient table-top setups

allowing noninvasive studies of low concentrated samples, regardless the solvent. Notably, we have shown above that TR-CD spectroscopy can provide an incisive tool for the study of charge localization in ruthenium complexes.

## 5. Concluding remarks

In this chapter, we have provided a general background of experimental techniques for transient absorption spectroscopy at different time scales. The research using these techniques is well developed, and a variety of applications has been demonstrated in the literature. The amount of information obtained from transient absorption is higher as compared to that available with time-resolved luminescence since it is possible to follow emissive and non-emissive species. Illustration of several applications of transient absorption to study dynamic processes occurring in inorganic coordination complexes has been presented. Particular attention has been paid to the investigation of photoinduced electron transfer in molecular and hybrid systems. This demonstrates transient absorption spectroscopy as a powerful tool for characterization of the dynamics of light-driven charge separation, one of the most important processes to understand and to optimize molecular systems for energy conversion. Furthermore, we highlight some recent developments related to transient absorption, including pump-pump-probe, circular dichroism or transient absorption spectroelectrochemistry. Development of advanced spectroscopic instruments based on transient absorption techniques is always in progress and will help to solve increasing scientific challenges in light-driven processes, particularly in the actual context of solar energy conversion.

## References

- [1] R. G. W. Norrish, G. Porter: Chemical Reactions Produced by Very High Light Intensities, *Nature* **164**, 658 (1949)
- [2] M. W. Windsor: Flash Photolysis and Triplet States and Free Radicals in Solution, *Photochem. Photobiol. Sci.* **2**, 455-458 (2003)
- [3] B. A. Thrush: The Genesis of Flash Photolysis, *Photochem. Photobiol. Sci.* **2**, 453–454 (2003)
- [4] N. Bloembergen: Nonlinear Optics and Spectroscopy, *Rev. Mod. Phys.* **54**, 685-695 (1982)
- [5] A. L. Schawlow: Spectroscopy in a New Light, *Rev. Mod. Phys.* **54**, 697-707 (1982)
- [6] A. H. Zewail: Femtochemistry: Atomic-Scale Dynamics of the Chemical Bond, *J. Phys. Chem. A* **104**, 5660–5694 (2000)
- [7] D. Strickland, G. Mourou: Compression of Amplified Chirped Optical Pulses, *Opt. Commun.* **55**, 447-449 (1985)
- [8] D. W. Thompson, A. Ito, T. J. Meyer:  $[\text{Ru}(\text{bpy})_3]^{2+*}$  and Other Remarkable Metal-Toligand Charge Transfer (MLCT) Excited States, *Pure Appl. Chem.* **85**, 1257–1305 (2013)
- [9] P. Dongare, B. D. B. Myron, L. Wang, D. W. Thompson, T. J. Meyer:  $[\text{Ru}(\text{bpy})_3]^{2+*}$  Revisited. Is It Localized or Delocalized? How Does It Decay?, *Coord. Chem. Rev.* **345**, 86-107 (2017)
- [10] N. H. Damrauer, G. Cerullo, A. Yeh, T. R. Boussie, C. V. Shank, J. K. McCusker: Femtosecond Dynamics of Excited-State Evolution in  $[\text{Ru}(\text{bpy})(3)](2+)$ , *Science* **275**, 54-57 (1997)

- [11] A. C. Bhasikuttan, M. Suzuki, S. Nakashima, T. Okada: Ultrafast Fluorescence Detection in Tris(2,2'-Bipyridine)Ruthenium(II) Complex in Solution: Relaxation Dynamics Involving Higher Excited States, *J. Am Chem. Soc.* **124**, 8398-8405 (2002)
- [12] A. Cannizzo, F. van Mourik, W. Gawelda, G. Zgrablic, C. Bressler, M. Chergui: Broadband Femtosecond Fluorescence Spectroscopy of [Ru(bpy)(3)](2+), *Angew. Chem. Int. Ed.* **45**, 3174-3176 (2006)
- [13] S. Campagna, F. Puntoriero, F. Nastasi, G. Bergamini, V. Balzani: Photochemistry and Photophysics of Coordination Compounds: Ruthenium. In: *Photochemistry and Photophysics of Coordination Compounds I*, doi:10.1007/128\_2007\_133, ed. by V. Balzani, S. Campagna (Springer Berlin Heidelberg, Berlin, Heidelberg 2007), pp. 117-214
- [14] A. Juris, V. Balzani, F. Barigelletti, S. Campagna, P. Belser, A. von Zelewsky: Ru(II) Polypyridine Complexes: Photophysics, Photochemistry, Electrochemistry, and Chemiluminescence, *Coord. Chem. Rev.* **84**, 85-277 (1988)
- [15] L. Striepe, T. Baumgartner: Viologens and Their Application as Functional Materials, *Chem. Eur. J.* **23**, 16924-16940 (2017)
- [16] K. Kitamoto, K. Sakai: Tris(2,2'-Bipyridine)Ruthenium Derivatives with Multiple Viologen Acceptors: Quadratic Dependence of Photocatalytic H<sub>2</sub> Evolution Rate on the Local Concentration of the Acceptor Site, *Chem. Eur. J.* **22**, 12381-12390 (2016)
- [17] Š. Lachmanová, G. Dupeyre, J. Tarábek, P. Ochsenein, C. Perruchot, I. Ciofini, M. Hromadová, L. Pospíšil, P. P. Lainé: Kinetics of Multielectron Transfers and Redox-Induced Structural Changes in N-Aryl-Expanded Pyridiniums: Establishing Their Unusual, Versatile Electrophoric Activity, *J. Am Chem. Soc.* **137**, 11349-11364 (2015)
- [18] D. L. Ashford, M. K. Gish, A. K. Vannucci, M. K. Brennaman, J. L. Templeton, J. M. Papanikolas, T. J. Meyer: Molecular Chromophore-Catalyst Assemblies for Solar Fuel Applications, *Chem. Rev.* **115**, 13006-13049 (2015)
- [19] G. Benkö, J. Kallioinen, J. E. I. Korppi-Tommola, A. P. Yartsev, V. Sundström: Photoinduced Ultrafast Dye-to-Semiconductor Electron Injection from Nonthermalized and Thermalized Donor States, *J. Am Chem. Soc.* **124**, 489-493 (2002)
- [20] B. Wenger, M. Grätzel, J.-E. Moser: Rationale for Kinetic Heterogeneity of Ultrafast Light-Induced Electron Transfer from Ru(II) Complex Sensitizers to Nanocrystalline TiO<sub>2</sub>, *J. Am Chem. Soc.* **127**, 12150-12151 (2005)
- [21] A. Hagfeldt, G. Boschloo, L. Sun, L. Kloo, H. Pettersson: Dye-Sensitized Solar Cells, *Chem. Rev.* **110**, 6595-6663 (2010)
- [22] S. Ardo, G. J. Meyer: Photodriven Heterogeneous Charge Transfer with Transition-Metal Compounds Anchored to TiO<sub>2</sub> Semiconductor Surfaces, *Chem. Soc. Rev.* **38**, 115-164 (2009)
- [23] S. Abbuzzetti, S. Bruno, S. Faggiano, E. Grandi, A. Mozzarelli, C. Viappiani: Time-Resolved Methods in Biophysics. 2. Monitoring Haem Proteins at Work with Nanosecond Laser Flash Photolysis, *Photochem. Photobiol. Sci.* **5**, 1109-1120 (2006)
- [24] R. Berera, R. van Grondelle, J. T. M. Kennis: Ultrafast Transient Absorption Spectroscopy: Principles and Application to Photosynthetic Systems, *Photosyn. Res.* **101**, 105-118 (2009)
- [25] G. Cerullo, C. Manzoni, L. Lüer, D. Polli: Time-Resolved Methods in Biophysics. 4. Broadband Pump-Probe Spectroscopy System with Sub-20 fs Temporal Resolution for the Study of Energy Transfer Processes in Photosynthesis, *Photochem. Photobiol. Sci.* **6**, 135-144 (2007)
- [26] P. Müller, K. Brettel: [Ru(bpy)<sub>3</sub>]<sup>2+</sup> as a Reference in Transient Absorption Spectroscopy: Differential Absorption Coefficients for Formation of the Long-Lived <sup>3</sup>MLCT Excited State, *Photochem. Photobiol. Sci.* **11**, 632-636 (2012)
- [27] K. Kalyanasundaram: Photophysics, Photochemistry and Solar Energy Conversion with Tris(Bipyridyl)Ruthenium(II) and Its Analogues, *Coord. Chem. Rev.* **46**, 159-244 (1982)
- [28] E. Terpetschnig, H. Szmecinski, H. Malak, J. R. Lakowicz: Metal-Ligand Complexes as a New Class of Long-Lived Fluorophores for Protein Hydrodynamics, *Biophys. J.* **68**, 342-350 (1995)

- [29] A. Brodeur, S. L. Chin: Ultrafast White-Light Continuum Generation and Self-Focusing in Transparent Condensed Media, *J. Opt. Soc. Am. B* **16**, 637-650 (1999)
- [30] F. Kanal, S. Keiber, R. Eck, T. Brixner: 100-kHz Shot-to-Shot Broadband Data Acquisition for High-Repetition-Rate Pump-Probe Spectroscopy, *Opt. Exp.* **22**, 16965-16975 (2014)
- [31] A. L. Dobryakov, S. A. Kovalenko, A. Weigel, J. L. Pérez-Lustres, J. Lange, A. Müller, N. P. Ernsting: Femtosecond Pump/Supercontinuum-Probe Spectroscopy: Optimized Setup and Signal Analysis for Single-Shot Spectral Referencing, *Rec. Sci. Instrum.* **81**, 113106 (2010)
- [32] G. P. Wakeham, K. A. Nelson: Dual-Echelon Single-Shot Femtosecond Spectroscopy, *Opt. Lett.* **25**, 505-507 (2000)
- [33] K. S. Wilson, C. Y. Wong: Single-Shot Transient Absorption Spectroscopy with a 45 ps Pump-Probe Time Delay Range, *Opt. Lett.* **43**, 371-374 (2018)
- [34] U. Megerle, I. Pugliesi, C. Schrieffer, C. F. Sailer, E. Riedle: Sub-50 fs Broadband Absorption Spectroscopy with Tunable Excitation: Putting the Analysis of Ultrafast Molecular Dynamics On solid Ground, *Appl. Phys. B* **96**, 215-231 (2009)
- [35] T. Nakayama, Y. Amijima, K. Ibuki, K. Hamanoue: Construction of a Subpicosecond Double-Beam Laser Photolysis System Utilizing a Femtosecond Ti:Sapphire Oscillator and Three Ti:Sapphire Amplifiers (a Regenerative Amplifier and Two Double Passed Linear Amplifiers), and Measurements of the Transient Absorption Spectra by a Pump-Probe Method, *Rev. Sci. Instrum.* **68**, 4364-4371 (1997)
- [36] C. Ruckebusch, M. Sliwa, P. Pernot, A. de Juan, R. Tauler: Comprehensive Data Analysis of Femtosecond Transient Absorption Spectra: A Review, *J. Photochem. Photobiol. Photochem. Rev.* **13**, 1-27 (2012)
- [37] M. Lorenc, M. Ziolk, R. Naskrecki, J. Karolczak, J. Kubicki, A. Maciejewski: Artifacts in Femtosecond Transient Absorption Spectroscopy, *Appl. Phys. B* **74**, 19-27 (2002)
- [38] K. Ekval, P. van der Meulen, C. Dhollande, L.-E. Berg, S. Pommeret, R. Naskrecki, J.-C. Mialocq: Cross Phase Modulation Artifact in Liquid Phase Transient Absorption Spectroscopy, *J. Appl. Phys.* **87**, 2340 (2000)
- [39] A. L. Dobryakov, J. L. P. Lustres, S. A. Kovalenko, N. P. Ernsting: Femtosecond Transient Absorption with Chirped Pump and Supercontinuum Probe: Perturbative Calculation of Transient Spectra with General Lineshape Functions, and Simplifications, *Chem. Phys.* **347**, 127-138 (2008)
- [40] R. Bonneau, J. Wirz, A. D. Zuberbuhler: Methods for the Analysis of Transient Absorbance Data, *Pure Appl. Chem.* **69**, 979-992 (1997)
- [41] I. H. M. v. Stokkum, D. S. Larsen, R. v. Grondelle: Global and Target Analysis of Time-Resolved Spectra, *Biochim. Biophys. Acta Bioenerg.* **1657**, 82-104 (2004)
- [42] S. Karlsson, J. Boixel, Y. Pellegrin, E. Blart, H.-C. Becker, F. Odobel, L. Hammarström: Accumulative Charge Separation Inspired by Photosynthesis, *J. Am Chem. Soc.* **132**, 17977-17979 (2010)
- [43] S. Mendes Marinho, M.-H. Ha-Thi, V.-T. Pham, A. Quaranta, T. Pino, C. Lefumeux, T. Chamaille, W. Leibl, A. Aukauloo: Time-Resolved Interception of Multiple Charge Accumulation in a Sensitizer-Acceptor Dyad, *Angew. Chem. Int. Ed.* **56**, 15936-15940 (2017)
- [44] M. H. Ha-Thi, V. T. Pham, T. Pino, V. Maslova, A. Quaranta, C. Lefumeux, W. Leibl, A. Aukauloo: Photoinduced Electron Transfer in a Molecular Dyad by Nanosecond Pump-Pump-Probe Spectroscopy, *Photochem. Photobiol.Sci.* **17**, 903-909 (2018)
- [45] T.-T. Tran, M.-H. Ha-Thi, T. Pino, A. Quaranta, C. Lefumeux, W. Leibl, A. Aukauloo: Snapshots of Light Induced Accumulation of Two Charges on Methylviologen Using a Sequential Nanosecond Pump-Pump Photoexcitation, *J. Phys. Chem. Lett.* **9**, 1086-1091 (2018)
- [46] M. Kuss-Petermann, O. S. Wenger: Pump-Pump-Probe Spectroscopy of a Molecular Triad Monitoring Detrimental Processes for Photoinduced Charge Accumulation, *Helv. Chim. Acta* **100**, e1600283 (2017)

- [47] J. Nomrowski, O. S. Wenger: Exploiting Potential Inversion for Photoinduced Multielectron Transfer and Accumulation of Redox Equivalents in a Molecular Heptad, *J. Am Chem. Soc.* **140**, 5343-5346 (2018)
- [48] M. Kuss-Petermann, M. Oraziotti, M. Neuburger, P. Hamm, O. S. Wenger: Intramolecular Light-Driven Accumulation of Reduction Equivalents by Proton-Coupled Electron Transfer, *J. Am Chem. Soc.* **139**, 5225-5232 (2017)
- [49] N. A. Besley, J. D. Hirst: Theoretical Studies toward Quantitative Protein Circular Dichroism Calculations, *J. Am Chem. Soc.* **121**, 9636-9644 (1999)
- [50] X. Xie, J. D. Simon: Picosecond Time-Resolved Circular Dichroism Spectroscopy: Experimental Details and Applications, *Rev. Sci. Instrum.* **60**, 2614-2627 (1989)
- [51] J. W. Lewis, R. A. Goldbeck, D. S. Kliger, X. Xie, R. C. Dunn, J. D. Simon: Time-Resolved Circular Dichroism Spectroscopy: Experiment, Theory, and Applications to Biological Systems, *J. Phys. Chem.* **96**, 5243-5254 (1992)
- [52] D. I. H. Holdaway, E. Collini, A. Olaya-Castro: Coherence Specific Signal Detection Via Chiral Pump-Probe Spectroscopy, *J. Chem. Phys.* **144**, 194112 (2016)
- [53] M. Anson, P. M. Bayley: Measurement of Circular Dichroism at Millisecond Time Resolution: A Stopped-Flow Circular Dichroism System, *J. Phys. E: Scientific Instruments* **7**, 481-486 (1974)
- [54] F. A. Ferrone, J. J. Hopfield, S. E. Schnatterly: The Measurement of Transient Circular Dichroism: A New Kinetic Technique, *Rev. Sci. Instrum.* **45**, 1392-1396 (1974)
- [55] J. Meyer-Ilse, D. Akimov, B. Dietzek: Ultrafast Circular Dichroism Study of the Ring Opening of 7-Dehydrocholesterol, *J. Phys. Chem. Lett.* **3**, 182-185 (2012)
- [56] K. Hiramatsu, T. Nagata: Broadband and Ultrasensitive Femtosecond Time-Resolved Circular Dichroism Spectroscopy, *J. Chem. Phys.* **143**, 121102 (2015)
- [57] A. Trifonov, I. Buchvarov, A. Lohr, F. Wuerthner, T. Fiebig: Broadband Femtosecond Circular Dichroism Spectrometer with White-Light Polarization Control, *Rev. Sci. Instrum.* **81**, 043104 (2010)
- [58] C. Niezborala, F. Hache: Measuring the Dynamics of Circular Dichroism in a Pump-Probe Experiment with a Babinet-Soleil Compensator, *J. Opt. Soc. Am. B* **23**, 2418-2424 (2006)
- [59] E. Chen, R. A. Goldbeck, D. S. Kliger: Nanosecond Time-Resolved Polarization Spectroscopies: Tools for Probing Protein Reaction Mechanisms, *Methods* **52**, 3-11 (2010)
- [60] L. Mangot, G. Taupier, M. Romeo, A. Boeglin, O. Cregut, K. D. H. Dorkenoo: Broadband Transient Dichroism Spectroscopy in Chiral Molecules, *Opt. Lett.* **35**, 381-383 (2010)
- [61] V. Stadnytskyi, G. S. Orf, R. E. Blankenship, S. Savikhin: Near Shot-Noise Limited Time-Resolved Circular Dichroism Pump-Probe Spectrometer, *Rev. Sci. Instrum.* **89**, 033104 (2018)
- [62] T. Dartigalongue, F. Hache: Observation of sub-100 ps Conformational Changes in Photolyzed Carbonmonoxy-Myoglobin Probed by Time-Resolved Circular Dichroism, *Chem. Phys. Lett.* **415**, 313-316 (2005)
- [63] M. Oppermann, B. Bauer, T. Rossi, F. Zinna, J. Helbing, J. Lacour, M. Chergui: Ultrafast Broadband Circular Dichroism in the Deep Ultraviolet, *Optica* **6**, 56-60 (2019)
- [64] H. Mesnil, M.-C. Schanne-Klein, F. Hache, A. Lemercier, C. Andraud: Experimental Observation of Nonlinear Circular Dichroism in a Pump-Probe Experiment, *Chem. Phys. Lett.* **338**, 269-276 (2001)
- [65] S. C. Bjorling, R. A. Goldbeck, S. J. Milder, C. E. Randall, J. W. Lewis, D. S. Kliger: Analysis of Optical Artifacts in Ellipsometric Measurements of Time-Resolved Circular Dichroism, *J. Phys. Chem.* **95**, 4685-4694 (1991)
- [66] J. Meyer-Ilse, D. Akimov, B. Dietzek: Recent Advances in Ultrafast Time-Resolved Chirality Measurements: Perspective and Outlook, *Laser Photonics Rev.* **7**, 495-505 (2013)
- [67] I. Bedja, S. Hotchandani, P. V. Kamat: Transient Absorption Spectroscopy of Nanostructured Semiconductor Films at Controlled Potentials. An in Situ Spectroelectrochemical Investigation of the Photosensitization Process, *J. Electroanal. Chem.* **401**, 237-241 (1996)

- [68] R. Lomoth, T. Häupl, O. Johansson, L. Hammarström: Redox-Switchable Direction of Photoinduced Electron Transfer in an Ru(bpy)<sub>3</sub><sup>2+</sup>–Viologen Dyad, *Chem. Eur. J.* **8**, 102-110 (2002)
- [69] S. Bold, L. Zedler, Y. Zhang, J. Massin, V. Artero, M. Chavarot-Kerlidou, B. Dietzek: Electron Transfer in a Covalent Dye–Cobalt Catalyst Assembly – a Transient Absorption Spectroelectrochemistry Perspective, *Chem. Comm.* **54**, 10594-10597 (2018)
- [70] V. Etacheri, C. Di Valentin, J. Schneider, D. Bahnemann, S. C. Pillai: Visible-Light Activation of TiO<sub>2</sub> Photocatalysts: Advances in Theory and Experiments, *J. Photochem. Photobiol. C: Photochem. Rev.* **25**, 1-29 (2015)
- [71] L. Hammarström: Accumulative Charge Separation for Solar Fuels Production: Coupling Light-Induced Single Electron Transfer to Multielectron Catalysis, *Acc. Chem. Res.* **48**, 840-850 (2015)
- [72] B. Bosnich: The Application of Exciton Theory to the Determination of the Absolute Configurations of Inorganic Complexes, *Acc. Chem. Res.* **2**, 266-273 (1969)
- [73] S. J. Milder, J. S. Gold, D. S. Kliger: Time-Resolved Circular Dichroism of the Lowest Excited State of (Δ)-Ru(bpy)<sub>3</sub><sup>2+</sup>, *Chem. Phys. Lett.* **144**, 269-272 (1988)
- [74] C. Niezborala, F. Hache: Excited-State Absorption and Circular Dichroism of Ruthenium(II) Tris(Phenanthroline) in the Ultraviolet Region, *J. Phys. Chem. A* **111**, 7732-7735 (2007)
- [75] A. T. Yeh, C. V. Shank, J. K. McCusker: Ultrafast Electron Localization Dynamics Following Photo-Induced Charge Transfer, *Science* **289**, 935-938 (2000)
- [76] A. Hauser, E. Krausz: The Excited-State Absorption of Ru(bpy)<sub>3</sub><sup>2+</sup> Reexamined, *Chem. Phys. Lett.* **138**, 355-360 (1987)
- [77] J. Applequist: A Full Polarizability Treatment of the π–π\* Absorption and Circular Dichroic Spectra of A-Helical Polypeptides, *J. Chem. Phys.* **71**, 4332-4338 (1979)
- [78] A. F. Fidler, V. P. Singh, P. D. Long, P. D. Dahlberg, G. S. Engel: Dynamic Localization of Electronic Excitation in Photosynthetic Complexes Revealed with Chiral Two-Dimensional Spectroscopy, *Nat. Commun.* **5**, 3286 (2014)
- [79] D. I. H. Holdaway, E. Collini, A. Olaya-Castro: Isolating the Chiral Contribution in Optical Two-Dimensional Chiral Spectroscopy Using Linearly Polarized Light, *Opt. Express* **25**, 6383-6401 (2017)